Chromatin enhancer activity of IκBα mediates the exit from naïve pluripotency

Luis G. Palma[1,2,3,δ], Daniel Álvarez-Villanueva[1,3,4,δ], María Maqueda[1,2,3], Mercedes Barrero[5], Arnau Iglesias[1,2,3], Joan Bertran[6], Damiana Álvarez-Errico[2], Carlos A. García-Prieto[2], Cecilia Ballaré[5], Virginia Rodriguez-Cortez[2], Clara Bueno[2], August Vidal[4], Alberto Villanueva[7], Pablo Menéndez[2,3,8,9,10], Gregoire Stik[2], Luciano Di Croce[5,10,11], Bernhard Payer[5,11], Manel Esteller[2,3,10,12], Lluís Espinosa[1,3,*] & Anna Bigas[1,2,3,*]

[1]Program in Cancer Research. Hospital del Mar Research Institute, Barcelona, Spain.

[2]Josep Carreras Leukemia Research Institute, Barcelona Spain.

[3]Centro de Investigación Biomédica en Red Cancer (CIBERONC), Madrid, Spain.

[4]Institut Investigació Biomèdica de Bellvitge (IDIBELL), L'Hospitalet de Llobregat, Barcelona, Spain.

[5]Centre for Genomic Regulation (CRG), The Barcelona Institute of Science and Technology, Barcelona, Spain.

[6]Faculty of Sciences, Technology and Engineering, Universitat de Vic - Universitat Central de Catalunya, Vic 08500 Spain

[7]Chemoresistance and Predictive Factors Group, Program Against Cancer Therapeutic Resistance (ProCURE), Catalan Institute of Oncology (ICO), Oncobell Program, Bellvitge Biomedical Research Institute (IDIBELL), L'Hospitalet de Llobregat, Barcelona, Spain.

[8]Spanish Network for Advanced Therapies (RICORS-TERAV). Carlos III Health Institute (ISCIII), Spain.

[9]Department of Biomedicine. University of Barcelona, Spain.

[10]Institucio Catalana de Recerca i Estudis Avançats (ICREA), Barcelona, Spain.

[11] Universitat Pompeu Fabra, Barcelona, Spain.

[12]Physiological Sciences Department, School of Medicine and Health Sciences, University of Barcelona (UB), Barcelona, Catalonia, Spain.

[δ]These authors contributed equally

Keywords: IκBα, NFKBIA, NF-κB, DNA Methylation, Polycomb, Embryonic Stem Cells, Pluripotency Exit, Germ Layer Specification,

*Corresponding authors:

Anna Bigas and Lluis Espinosa

Cancer Research Program. CIBERONC.

Hospital del Mar Research Institute

Doctor Aiguader 88, 08003, Spain.

Tel: +34 933160440; email: abigas@researchmar.net; lespinosa@researchmar.net

Summary

Inflammatory signals are key in development and cell differentiation, yet their precise involvement in the transition from naïve to primed pluripotency remains elusive. One of the main sensors of inflammation in cells is the IκBα protein which exerts its function through activation of NF-κB. Our previous work identified a chromatin role of IκBα that is crucial for the proper regulation of different tissue stem cells. Here, we demonstrate that IκBα depletion causes profound epigenetic rewiring in pluripotent stem cells characterized by altered histone post-translational modifications and DNA methylation, which is associated with changes in transcriptional regulation. These changes led to stabilization of cells in a ground state of naïve pluripotency when cultured in Serum/LIF conditions and differentiation impairment. Mechanistically, IκBα binds to intergenic chromatin regions in the naïve pluripotency state, which result in altered activation status of a subset of enhancers, including several associated to pluripotency-related genes. Through the engineering of separation-of-function mutants, we demonstrate that the effects of IκBα in the regulation of stem cell pluripotency are NF-κB-independent, but mainly relies on its chromatin-related function. Altogether, our results highlight a novel mechanism by which IκBα participates in regulating the pluripotent states of embryonic stem cells, shedding light on the interplay between inflammatory signals and pluripotency regulation.

52 **INTRODUCTION**

53 Embryonic Stem Cells (ESCs) pluripotency is characterized by the capacity to generate all
54 somatic and germline lineages both *in vitro* and *in vivo*, depending on the culture conditions.
55 When cultured in serum plus Leukemia Inhibitory Factor (LIF) (Serum/LIF), murine ESCs
56 (mESCs) include cells interconverting to different metastable states [1] that either resemble
57 preimplantation blastocyst (naïve pluripotency) or post-implantation (primed pluripotency)
58 embryonic stages [2–5]. The heterogeneity of mESCs in Serum/LIF is reduced by culturing them
59 in the presence of GSK3β and MEK1/2 inhibitors (CHIR99021 and PD0325901, respectively)
60 along with LIF (2i/LIF). Under these conditions, mESCs enter a ground state of naïve
61 pluripotency characterized by self-renewal activity while suppressing any pro-differentiating
62 signals [6,7]. This pluripotent state closely resembles the inner cell mass of the E4.0 mouse
63 preimplantation blastocyst [8]. After implantation, pluripotent capability of the mouse embryo
64 (E5.5) becomes restricted to Epiblast Stem Cells (EpiSCs), which represent a primed
65 pluripotent state, characterized by coexpression of pluripotency and lineage specification
66 markers [9,10]. EpiSCs can give rise to cells of the three different germ layers (endoderm,
67 mesoderm and ectoderm), albeit their contribution to chimeras or to germ cells is greatly
68 compromised [4,11]. EpiSCs can be derived *in vitro* from naïve pluripotent cells cultured in a
69 medium supplemented with Nodal and fibroblast growth factor (FGF) [12]. Different epigenetic
70 features distinguish naïve from primed pluripotent states [13], such as changes in the X
71 chromosome inactivation in female cells [12,14], histone post-translational modifications [10] or a
72 global DNA hypomethylation profile observed in naïve pluripotent stem cells [15–17]. These
73 epigenetic changes are a prerequisite for the subsequent activation of gene circuits
74 associated with pluripotency exit and germ layer specification [9,10]. Crucial regulatory elements
75 for the transition from naïve to primed pluripotency state are located in distal DNA regions or
76 enhancers to facilitate the resolution toward the primed state [18,19]. Therefore, identifying
77 novel players to fine-tune the equilibrium between ground and primed states is crucial for
78 preserving both pluripotency stability and differentiation capability in mESCs.

79 Inflammation is a defense mechanism mostly activated in response to harmful endogenous
80 or foreign stimuli, which involves different signaling pathways including NF-κB. Canonical NF-
81 κB signaling is triggered by the IKK kinase complex, which induce the phosphorylation and
82 subsequent degradation of the NF-κB inhibitor, IκBα, leading to nuclear translocation of the
83 NF-κB factors (e.g. p50/p65) [20]. We have previously identified an alternative nuclear function
84 of IκBα involving the interaction with histone deacetylases (HDACs), core elements of the
85 Polycomb Repressor Complex 2 (PRC2) and histones [21–23]. This nuclear IκBα function is crucial
86 for tissue stem cell homeostasis and the proper differentiation of epidermal, intestinal and
87 hematopoietic cells [22–25].

88 There is now robust evidence that inflammatory signals are crucial in stem cell development
89 [26,27], and it was recently demonstrated that attenuation of inflammatory signals by ATG5
90 facilitates mESCs differentiation [28]. Unexpectedly, being NF-κB pathway a pivotal regulator of

inflammation, classical NF-κB factors including p50 and RelA/p65 are expressed at very low levels in mESCs. Overexpression of NF-κB proteins leads to cell differentiation while expression of the IκBα super-repressor (S32-36A mutant) increases expression of pluripotency markers [29]. Similarly, inhibition of Protein Kinase C (PKC) activity in mESCs, which in turn restrains NF-κB signaling, allows keeping mESCs in a ground pluripotency state, thus facilitating the generation of induced pluripotent stem cells (iPSCs) [30]. Together these results indicate that NF-κB inhibition is required for maintaining the pluripotent state of murine ESCs. Given the importance of NF-κB in the multiple aspects of stem cell biology [31] and the pivotal role of IκBα in NF-κB regulation, the possible impact of the IκBα chromatin function in cell fate has remained challenging.

We have now investigated the role of IκBα in a context of pluripotent stem cells. Unexpectedly, and in contrast with the pro-differentiation effects of NF-κB activation, depletion of the NF-κB inhibitor IκBα precludes the exit of mESCs from naïve pluripotency associated with an epigenetic rewiring. By using the recently described Separation-Of-Function (SOF) IκBα mutants [32], we have now demonstrated that pluripotency regulation by IκBα is mainly exerted through its chromatin-related function but independent on its capacity to negatively regulate NF-κB.

RESULTS

IκBα accumulates in the chromatin of naïve pluripotent cells

Because of the prominent role of NF-κB signaling in mESCs regulation, we analyzed the expression pattern of the different NF-κB members including the IκB inhibitors in the three defined pluripotent stages: ground state of naïve pluripotency (2i/LIF), naïve pluripotency (Serum/LIF), and primed pluripotency (Epiblast Stem Cells or EpiSCs) (Figure 1A). In agreement with NF-κB being a pro-differentiation factor, canonical NF-κB inhibitors including IκBα (*Nfkbia*), IκBβ (*Nfkbib*) and IκBε (*Nfkbie*) were all expressed in the naïve pluripotency state (both ground and Serum/LIF), with *Nfkbia* levels significantly reduced upon naïve pluripotency exit towards EpiSCs (Figure 1B). In contrast, *Rela, Nfkb1 and Nfkb2 genes* codifying for the NF-κB factors p65/RelA, p105 and p100, respectively, showed an opposite pattern and either increased or maintained their levels in EpiSCs (Figure 1C). We further characterized the distribution of IκBα in the cytoplasm, nucleus and chromatin fractions of the three states of pluripotency (Figure 1D). IκBα protein levels in the cytoplasm and the nucleus correlated with the detected RNA levels in the three different cellular states being highest in 2i/LIF condition (Figure 1B). Interestingly, a notable accumulation of IκBα was observed in the chromatin of naïve pluripotent cells cultured in Serum/LIF conditions compared to 2i/LIF. In contrast, IκBα was entirely absent from the chromatin of EpiSCs. (Figure 1D). The abundance of IκBα RNA and protein in the context of naïve pluripotency compared to EpiSCs was further corroborated through analysis of an additional database encompassing both naïve and primed pluripotent states [33] (Figure 1E).

Next, we studied IκBα expression in differentiated embryoid bodies (EBs) from mESCs (Serum/LIF) (see materials and methods) and analyzed the expression levels of different pluripotency (*Dppa4, Pou5f1, Sox2, Prdm14, Klf4, Zfp42 [Rex1], Nanog*), differentiation-linked (*Mesp1, Gata6, Lhx1, Gata4, Wnt3a, Fgf5, Nes, Axin2, Wnt3, Eomes, T, Foxa2, Mixl1, Lef1*), and NF-κB genes (*Nfkbid, Nfkbia, Nfkbie, Nfkbib, Nfkbiz, Rel, Rela, Relb*) by RNA sequencing. *Nfkbia* (IκBα gene) was expressed at higher levels specifically in mESCs (Serum/LIF) whereas cells undergoing differentiation (48h and 96h) displayed a reduction in its expression levels (Figure 1F). The expression pattern of *Nfkbia* was similar to the pluripotency genes, whereas most of the NF-κB genes were upregulated upon differentiation, clustering together with developmental genes, as previously described [29].

Taken together, these data show that the expression of *Nfkbia*, like the other *Nfkbi*, is high in the naive pluripotent state, in contrast to the NF-κB genes, which cluster together with differentiation markers. In addition, IκBα accumulates in the chromatin of naive pluripotent cells, more so in cells cultured under serum/LIF.

Lack of IκBα impairs the exit from the naïve pluripotency state

144 To investigate the functional implication of the chromatin accumulation of IκBα in naïve
145 pluripotency, we knocked-out IκBα protein in mESCs by CRISPR-Cas9 (IκBα-KO mESCs) (Figure
146 1G and materials and methods). We did not detect major changes in NF-κB target genes upon
147 IκBα depletion neither in mESCs, nor 48h and 96h EBs (Figure 1H), suggesting that NF-κB
148 regulation did not require IκBα at this stage or it might be compensated by the other canonical
149 or non-canonical IκBs (IκBβ, IκBε or p100), as previously demonstrated [34,35]. Paradoxically,
150 IκBα-KO mESCs have an impaired capability to undergo differentiation, since IκBα-KO EBs
151 cannot properly evolve towards differentiation trajectories (Figure 2A). This observation was
152 confirmed by analysis of naïve pluripotency markers at 96h (*Gab1, Sox2, Esrrb, Zfp42, Dppa4,*
153 *Klf2, Prdm14, Klf4, Tfcp2l1*), which displayed higher expression levels in IκBα-KO compared
154 to their wild-type (IκBα-WT) counterparts (Figures 2B and S1A). Differentiation of IκBα-KO EBs
155 was deficient in programs associated with all germ layer specification (endoderm, mesoderm,
156 and ectoderm) (Figures 2C-E). Moreover, IκBα-KO EBs were smaller in size (Figure S1B), and
157 maintained higher expression of the pluripotency program even at 216h (Figures 2F and S1C).
158 We also detected a higher number of Alkaline Phosphatase-expressing cells (Figures 2G and
159 S1D) and higher expression of the pluripotency marker SSEA-1 (Figure S1E) at 216h IκBα-KO
160 EBs. To further study the requirement of IκBα in pluripotency exit *in vivo*, we established
161 teratomas by subcutaneous injection of IκBα-WT and IκBα-KO mESCs (Figure S1F and
162 materials and methods) in NSG (NOD.Cg-Prkdc^{scid} Il2rg^{tm1Wjl}/SzJ) mice. IκBα-KO teratomas
163 showed a decreased differentiation potential, as indicated by higher number of OCT4^{+} cells
164 (Figures S1G-H). These observations underscore the essential role of IκBα in the exit from the
165 pluripotency state in mouse embryonic stem cells (mESCs).

166 To determine the specific time-point in which IκBα is required for pluripotency exit, we
167 differentiated IκBα-WT and IκBα-KO mESCs cultured in Serum/LIF (naïve pluripotency)
168 towards EpiSCs (primed pluripotency) for 120h (Figure 2H and materials and methods). IκBα-
169 KO cells were not committed towards the primed pluripotency stage and maintained an
170 elevated expression levels of naïve pluripotency genes (*Dppa3, Nanog, Sox2, Rex1, Klf2, Klf4,*
171 *Gbx2, Tbx3*) (Figure 2I). Additionally, IκBα-KO cells retained a naïve pluripotent morphology,
172 forming tight clusters and resembling cells cultured in 2i/LIF medium (Figure S1I). These data
173 demonstrate that IκBα is required for the exit of the naïve state of pluripotency and its
174 deficiency results in impaired differentiation of mESC *in vivo* and *in vitro*, without imposing
175 major changes in the regulation of canonical NF-κB.

176 **IκBα-KO mESCs resemble the ground-state of naïve pluripotency under Serum/LIF**
177 **conditions**

178 As mentioned, mESCs cultured in serum/LIF are highly heterogeneous, containing a mixture
179 of cell states that resemble developmental transitions from preimplantation (naïve
180 pluripotency) to postimplantation (primed pluripotency) embryo [2,3]. To investigate how IκBα
181 deficiency was affecting the exit of mESCs from naïve pluripotency, we performed a Gene Set
182 Enrichment Analysis (GSEA) using RNA-seq data from IκBα-KO and IκBα-WT mESCs cultured

183 in Serum/LIF against gene signatures for ground (2i/LIF) and naïve (Serum/LIF) pluripotency
184 [36]. GSEA results revealed a significant enrichment in Serum/LIF IκBα-KO mESCs transcriptome
185 for genes specifically expressed in the ground state (2i/LIF), while they negatively correlate
186 with mESCs cultured in Serum/LIF (Figure 3A) [36]. Specifically, IκBα-KO mESCs expressed higher
187 levels of the ground state pluripotency genes *Klf2, Nanog, Pou5f1, Prdm14, Gbx2, Tbx3,*
188 *Zfp42[Rex1]* and *Klf4* (Figure 3B), similar to IκBα-WT mESCs cultured in 2i/LIF (Figure S2A).
189 Since ground (2i/LIF) and naïve (Serum/LIF) states are characterized by important differences
190 in epigenetic marks, we carried out an epigenetic profiling of IκBα-WT and IκBα-KO mESCs
191 cultured in Serum/LIF. We performed chromatin immunoprecipitation followed by
192 sequencing (ChIP-seq) of histone modifications associated to gene activation (H3K4me3),
193 gene repression (H3K27me3) and constitutive heterochromatin (H3K9me3) (Figures 3C-D and
194 S2B-D). Overall, Serum/LIF IκBα-KO mESCs exhibited a more permissive chromatin status as
195 evidenced by increased H3K4me3 and decreased H3K9me3 levels, while H3K27me3 was
196 redistributed in both directions (Figure 3C). Notably, the gain in H3K4me3 mark was
197 associated with a reduction of H3K27me3 levels in genes associated with naïve pluripotency
198 (Figures 3C-D and S2B-C), in agreement with the higher pluripotent state observed in IκBα-
199 KO mESCs. As mentioned, detection of the H3K9me3 mark was significantly reduced in IκBα-
200 KO mESCs (Figures 3C and S2D). These regions correspond to genes involved in DNA
201 methylation and chromatin edition functions (Figure 3C). By analyzing the DNA methylation
202 status under Serum/LIF conditions by immunofluorescence of 5-methyl-cytosine (5mC) we
203 found a global DNA hypomethylation in IκBα-KO mESCs (Figure 3E), which is one of the key
204 features of the ground state of naïve pluripotency (2i/LIF) [15,37]. To further characterize the
205 DNA methylation status in IκBα-KO cells, we performed DNA methylation arrays [38] in IκBα-
206 KO and IκBα-WT mESCs (Serum/LIF) and 96h after EB differentiation. We observed a strong
207 reduction of the DNA methylation level in IκBα-KO mESCs in a genome-wide fashion (Figure
208 3F). Specifically, IκBα-KO mESCs contain lower DNA methylation levels in promoters, gene
209 bodies, enhancers and imprinted regions (Figure 3G), and this DNA hypomethylation status
210 was not associated with any particular chromosome (Figure S2E). DNA hypomethylation was
211 maintained upon 96h in IκBα-KO EBs (Figures 3F-G and S2F).

212 These results further indicate that IκBα is required for the transition from ground to primed
213 pluripotent states and for the proper regulation of the histone post-translational
214 modifications (PTMs) and DNA methylation changes associated with this process. We propose
215 that the enhanced pluripotent state found in IκBα-KO mESCs under basal conditions
216 (Serum/LIF) may negatively impact on their differentiation potential, similar to that described
217 for other models with stabilized naïve pluripotent state [39,40].

218 **IκBα binds to intergenic regions to attenuate the activation status of chromatin linked to**
219 **naïve pluripotency genes**

220 To gain insight into the mechanism by which IκBα regulates the transition from naïve to
221 primed pluripotent states, we knocked-in a 3xFLAG-tag into the IκBα locus and used these

222 transgenic cells for ChIP-seq assay with the anti-FLAG antibody (see Materials and Methods).
223 We identified 817 bona-fide IκBα-bound chromatin regions which were consistent between
224 three independent replicates (Figure S3A). Among all the genome regions, IκBα was mainly
225 bound to distal intergenic and intronic regions (38.5% and 42.2% of total IκBα peaks,
226 respectively) (Figure 4A). Interestingly, IκBα-bound regions coincide with those that gain
227 enhancer activation-related H3K27Ac signals in EpiSCs (Figures S3B-C). The fact that IκBα was
228 released from chromatin at the stage of primed pluripotency (Figure 1D) suggested that IκBα
229 might be involved in fine-tuning these regions at the exit from naive pluripotency. To address
230 this question, we quantified the total amount of H3K27Ac (active enhancer) by western blot
231 analysis of chromatin extracts of IκBα-WT and IκBα-KO mESCs cultured in Serum/LIF. We
232 observed an increase of this activation mark in IκBα-KO mESCs, whereas we did not observe
233 global changes in H3K4me1 levels, a marker of poised enhancers (Figures S3D-E). These
234 results suggested that IκBα depletion in naïve pluripotency might lead to an increase in the
235 global levels of active enhancers, which are characterized by a gain of H3K27Ac without
236 changes in H3K4me1 levels [41]. The increase in H3K27Ac was further validated by ChIP-seq
237 experiments conducted in both IκBα-WT and IκBα-KO mESCs. Notably, depletion of IκBα
238 protein under Serum/LIF conditions led to an increase in the deposition of H3K27Ac at regions
239 where we detected IκBα binding (Figure 4B), while levels of H3K4me1 were not generally
240 altered. Since IκBα deficiency was affecting enhancer-related histone marks, we further
241 profiled the enhancer status of IκBα-KO mESCs by analyzing the differential distribution of
242 poised enhancers (showing changes in H3K4me1 levels without affecting H3K27Ac) and active
243 enhancers (chromatin regions decorated with H3K4me1 that also display H3K27ac binding)
244 (Figures 4D). Overall, IκBα-KO mESCs showed a reduction in poised enhancers at genes (or
245 related genomic regions) associated to differentiation processes (Figures 4D and S3F),
246 whereas active enhancers of genes associated to pluripotency were significantly enriched
247 (Figures 4D-E and S3G). These results further support that mESCs lacking IκBα are
248 epigenetically reinforced in the ground state of naïve pluripotency. Since the majority of IκBα
249 chromatin peaks were located in distal intergenic and intronic regions (Figure 4A), and we
250 found that IκBα deficiency led to changes in the enhancer status (Figure 4D), we took
251 advantage of publicly available Hi-C data to identify topologically associating domains (TADs)
252 at putative IκBα target genes in Serum/LIF mESCs [42]. It was previously demonstrated that TADs
253 are organized in distinct chromatin compartments defined as active (Compartment A) or
254 inactive (Compartment B) [43]. Importantly, chromatin regions bound by IκBα mainly
255 correspond to TADs of the active compartment (81%), whereas a small proportion of IκBα
256 peaks were found in inactive chromatin (19%) (Figure S3H). Furthermore, TADs harboring IκBα
257 binding exhibited a greater proportion of enhancers differentially regulated in IκBα-KO cells
258 when compared to all TADs (92% vs. 74%, respectively) (Figure S3H). Additionally, genes
259 located within TADs bound by IκBα are predominantly associated with mechanisms linked to
260 pluripotency identity (data not shown). To address the functional relevance of this
261 observation, we investigated the expression pattern of pluripotency-related genes in IκBα-
262 WT and IκBα-KO mESCs at naïve pluripotency (cultured in Serum/LIF) and differentiation (48h

263 EBs) stages (Figure 4F). Most of the genes analyzed were significantly upregulated in IκBα-KO
264 mESCs, and this difference was further accentuated in IκBα-KO 48h EBs. These results suggest
265 that IκBα modulates the dinamyc expression of pluripotency genes through a distal regulatory
266 mechanism involving enhancer activity and 3D chromatin architecture. To address this
267 hypothesis, we crossed Hi-C data with ChIP-seq of IκBα and enhancer-related histone marks
268 (H3K27Ac and H3K4me1), together with RNA-seq data. In this meta-analysis, we identified a
269 TAD region encompassing the Tbx3 locus with IκBα binding sites (Figure 4G). Interestingly, we
270 observed that the IκBα-bound regions interact with the region containing Tbx3 gene (Figure
271 4G; interactions highlighted with an arrow in the contact map). Moreover, that region harbors
272 an active enhancer marked by H3K27Ac/K4me1, whose activation status is heightened in
273 IκBα-KO mESCs, likely participating in increased expression of the Tbx3 gene (Figure 4G,
274 bottom panel) and other interactions are detected between the differentially activated
275 enhancer and the Tbx3 locus in this TAD (Figure 4G, interaction highlighted with a gray arrow
276 in the contact map).

277 We then determined whether differential enhancer activation status observed in IκBα-KO
278 mESCs (evidenced by increased H3K27Ac) was reversible. We engineered a doxycycline-
279 inducible IκBα construct and introduced it into IκBα-KO mESCs. Treatment of these cells with
280 doxycycline for several passages under Serum/LIF conditions (i-IκBα^{WT} mESCs, Figure 4H) led
281 to sustained IκBα expression and a significant reduction of global levels of H3K27Ac (Figures
282 4I and S3I). Ectopic expression of i-IκBα^{WT} in mESCs was also sufficient to attenuate the
283 expression of the naïve pluripotency genes *Zfp42, Klf2, Sox2* and *Tbx3 in* IκBα-KO mESCs under
284 Serum/LIF conditions (Figure S3L).

285 **IκBα attenuates the activation of intergenic regions in an NF-κB independent manner**

286 Uncovering the actual impact of chromatin-related IκBα function is challenging due to the
287 predominant role of this protein on NF-κB regulation. Recent work from our group has
288 identified the residues in the IκBα protein critical for NF-κB-binding or chromatin-binding
289 through H2A/H4. Mutation of these residues, allows to specifically discriminate between
290 either of the two functions of IκBα [32]. We generated doxycycline-inducible constructs to
291 express separation-of-function (SOF) IκBα mutants: i) exclusively interacts with NF-κB and is
292 deficient for chromatin binding (i-IκBα$^{\Delta Chromatin}$) or ii) interacts with histones but is deficient
293 for NF-κB interaction and inhibition (i-IκBα$^{\Delta NF\text{-}\kappa B}$) (Figure 5A). We introduced one of the SOF
294 IκBα mutants into IκBα-KO mESCs and confirmed their functionality by pull-down
295 experiments. We found that i-IκBα$^{\Delta NF\text{-}\kappa B}$ was able to interact with histone H2A but not with
296 the NF-κB member p50 and, i-IκBα$^{\Delta Chromatin}$ could interact with p50 but not with H2A, while i-
297 IκBα^{WT} preserved all interactions (Figures 5B-C). Importantly, when we induced the three
298 different IκBα forms (i-IκBα^{WT}, i-IκBα$^{\Delta NF\text{-}\kappa B}$ and i-IκBα$^{\Delta Chromatin}$, Figure S4A), only i-IκBα^{WT} and i-
299 IκBα$^{\Delta NF\text{-}\kappa B}$ were found in the chromatin fraction of mESCs, whereas IκBα$^{\Delta Cromatin}$ was retained
300 in the cytoplasm (Figures 5D and S4B). To address whether IκBα was participating in the
301 stabilization of the ground-state of naïve pluripotency in an NF-κB-independent manner, we

302 studied which of the SOF mutants (IκBα$^{\Delta NF\text{-}\kappa B}$ or IκBα$^{\Delta Chromatin}$) was able to reverse the
303 phenotype of IκBα-KO mESCs (Figure S4C). We observed the reduction of the global levels of
304 H3K27Ac upon induction of i-IκBα^{WT} and i-IκBα$^{\Delta NF\text{-}\kappa B}$, but not of IκBα$^{\Delta Chromatin}$ (Figures 5E and
305 S4D). Similarly, induction of IκBα$^{\Delta NF\text{-}\kappa B}$ was enough to reduce the H3K27Ac amount in
306 enhancers with increased H3K27Ac in IκBα-KO mESCs, but not when IκBα$^{\Delta Chromatin}$ was
307 expressed (Figure 5F). Interestingly, H3K4me1 levels followed a similar pattern as H3K27Ac in
308 those specific loci, and a significant reduction was achieved upon IκBα$^{\Delta NF\text{-}\kappa B}$ overexpression,
309 whereas IκBα$^{\Delta Chromatin}$ was mediating an opposite effect (Figure 5G). In addition, the ground
310 state-associated DNA hypomethylation was reverted in i-IκBα^{WT} and i-IκBα$^{\Delta NF\text{-}\kappa B}$ mESCs but
311 not in i-IκBα$^{\Delta Chromatin}$ mESCs (Figure 5H). Furthermore, the naïve pluripotent gene expression
312 (*Zfp42, Klf2, Sox2*, *Tbx3*) was reduced upon inducing i-IκBα$^{\Delta NF\text{-}\kappa B}$, while induction of i-
313 IκBα$^{\Delta Chromatin}$ resulted in their increase (Figure S4E).

314 To address whether reverting to the basal epigenetic status is enough to rescue the
315 differentiation capability, i-IκBα^{WT}, i-IκBα$^{\Delta NF\text{-}\kappa B}$ and i-IκBα$^{\Delta Chromatin}$ mESCs were differentiated
316 into EBs (Figure S4C). Induction of IκBα^{WT} and IκBα$^{\Delta NF\text{-}\kappa B}$ was enough to restore the
317 differentiation potential of IκBα-KO mESCs, since the number of differentiated cells (based on
318 percentage of SSEA-1^{neg} cells) increased (Figures 5I and S4F). Moreover, we found a reduced
319 number of AP+ colonies from 216h IκBα-KO EBs after induction of i-IκBα^{WT} and i-IκBα$^{\Delta NF\text{-}\kappa B}$,
320 similar to the number of colonies obtained from IκBα-WT EBs (Figures 5J and S4G). Lastly,
321 the number of remaining pluripotent-like cells (defined by OCT3/4 NANOG staining) was also
322 reduced in i-IκBα^{WT} and i-IκBα$^{\Delta NF\text{-}\kappa B}$ 216h EBs, and only small and few regions of
323 undifferentiated cells was observed (Figures 5K and S4H). On the other hand, induction of i-
324 IκBα$^{\Delta Chromatin}$ did not restore the differentiation potential of IκBα-KO mESCs, and phenocopied
325 the differentiation defects observed in IκBα-depleted mESCs.

326 These results demonstrate that the chromatin-dependent IκBα function, but not its NF-κB-
327 related activity, is necessary and sufficient to revert the stabilization in the ground state of
328 naïve pluripotency correlating with higher DNA methylation and lower H3K27Ac levels. Our
329 results demonstrate that the chromatin function of IκBα alters the activation status of
330 enhancers, which impacts the expression of genes involved in the maintenance of the naïve
331 pluripotency. This function is independent of the NF-κB-inhibitory activity of IκBα.

DISCUSSION

Here we have identified a new and unexpected function for the IκBα protein in the regulation of the naïve pluripotency exit. Using mESCs to investigate the role of IκBα in pluripotency maintenance and differentiation, we discovered that the absence of IκBα severely impairs the exit of pluripotency. Furthermore, IκBα-KO mESCs stabilizes the ground state of naïve pluripotency under Serum/LIF conditions, shedding light on its function as a critical regulator of the transition from naïve to primed pluripotency. While IκBα is commonly known for its role as an inhibitor of the NF-κB signaling pathway [20], our laboratory has previously furnished compelling evidence of its alternative role through its interaction with histones and other chromatin components [21–23]. We have demonstrated that chromatin-bound IκBα plays a crucial role in regulating skin and intestinal stem cells [22,24], hematopoietic stem cell development [25], and it influences the regenerative capacity of these tissues, and in some cases, their susceptibility to neoplastic transformation. Disentangling the chromatin-related function of IκBα from its canonical role as an inhibitor of NF-κB has been challenging, making it difficult to determine its truly biological significance. To tackle this challenge, we engineered separation-of-function (SOF) mutants of IκBα, as detailed in [44], by identifying specific residues that are essential for binding either NF-κB elements or histones. Interestingly, we have shown that only the histone-binding proficient IκBα mutant (IκBα$^{\Delta NF\text{-}\kappa B}$), which lacks the ability to bind to NF-κB, has the capability to reverse the stabilization of the ground state observed in IκBα-KO mESCs. This is sufficient to facilitate their exit from the state of naïve pluripotency, restoring their full differentiation potential (Figure 5). The involvement of NF-κB in pluripotency has been a subject of prior investigation. Studies have revealed that pluripotent cells display a dampened inflammatory signaling pathway, which is induced upon pluripotency dissolution and activation of differentiation [29,45]. However, the precise molecular mechanisms underlying the attenuated status of NF-κB during this stage remain incompletely understood. A recent work has shed light on a potential regulatory axis involving ATG5-β-TrCP1-NF-κB, proposing it as a mechanism that diminishes NF-κB activity by stabilizing the IκBα protein in mESCs [28]. In any case, since modification of canonical NF-κB activity directly impacts on the levels IκBα expression, the previous NF-κB-associated phenotypes should be reevaluated considering this chromatin role of IκBα. Furthermore, the expression of IκBα$^{\Delta Chromatin}$, which retains the inhibitory function of NF-κB, failed to mitigate the ground state stabilization observed in IκBα-KO mESCs (Figure 5). This finding suggests that the observed role of IκBα in regulating the exit from naïve pluripotency is not due to NF-κB inhibition. In fact, there is evidence that the chromatin function of IκBα is an ancestral function preceding its role as NF-κB inhibitor. In Caenorhabditis Elegans (*C.elegans*), which lacks NF-κB orthologs but possesses two homologs of IκBα, the absence of IκBα orthologs has severe multi-organ differentiation defects [46]. This observation further supports the notion that the chromatin-related function of IκBα plays a fundamental role in developmental processes, independent of its canonical role in NF-κB signaling.

371 We have observed that IκBα-KO mESCs exhibit epigenetic and transcriptomic profiles
372 resembling the ground state of naïve pluripotency under Serum/LIF culture (Figure 3). In this
373 regard, the fact that IκBα is preferentially located in the chromatin of mESCs cultured in
374 Serum/LIF, when they exhibit a high degree of heterogeneity, suggests that IκBα might act as
375 a regulator of this heterogeneity. One potential explanation might be that IκBα could be
376 affecting the stability of fluctuating transcription factors, which is crucial to mediate the
377 pluripotent-to-differentiation balance [3]. Thus, the lack of IκBα might stabilize those
378 transcription factors that would favor the ground-state observed in IκBα-KO mESCs cultured
379 in Serum/LIF. Further experiments are required to demonstrate this hypothesis. Moreover,
380 the differences in murine and human pluripotency [11] point out the necessity to address the
381 real impact of IκBα modulation in the stabilization of the ground state in human pluripotent
382 stem cells. Our investigation has also revealed that IκBα accumulates in the intergenic
383 chromatin regions of naïve pluripotent cells (Figures 1D and 4A). Mechanistically, this binding
384 of IκBα serves to safeguard enhancers associated with pluripotency from excessive activation.
385 This is evidenced by the higher abundance of active enhancers observed in IκBα-depleted
386 mESCs, particularly in regions linked to pluripotency located within TADs where IκBα is bound.
387 A recent study highlights the significance of maintaining a proper 3D chromatin architecture
388 during the resolution of the naïve pluripotent state [47]. Our findings suggest that IκBα may
389 potentially influence the 3D conformation of regions relevant to pluripotency, thereby fine-
390 tuning the expression of genes crucial for sustaining naïve pluripotency (Figure 6).
391 Nevertheless, the precise mechanisms by which the absence of IκBα impacts 3D chromatin
392 architecture remain to be elucidated.

393 In summary, our work establishes that IκBα mediates the exit from naïve pluripotency by
394 modulating the activation of enhancers associated with pluripotency genes. Importantly, this
395 newly identified role of IκBα operates independently of its canonical function in inhibiting the
396 NF-κB pathway. Our findings underscore the intricate interplay between inflammation and
397 pluripotency status, revealing a previously unrecognized complexity in their interaction.

398 **METHODS**

399 **Cell culture**

400 mESC line ES-E14TG2a (ATCC; Cat #CRL-1821) was cultured on plastic dishes precoated with
401 0.1% (w/v) Gelatin (Sigma; Cat #G2500-100G) in Serum/LIF medium. Serum/LIF is composed
402 by DMEM basal medium (Sigma-Aldrich; Cat #D5796) supplemented with 15% FBS (ESC-
403 qualified; Gibco Cat #26140079), 1X Glutamax (Gibco; Cat #35050061), 1X NEAA (Gibco;
404 Cat#11140050), 1mM Sodium Pyruvate (Gibco; Cat#11360070), 1000U/mL Leukemia
405 Inhibitory Factor (LIF) (Millipore, Cat #ESG1107) and 0.125mM 2-mercaptoethanol (Gibco;
406 Cat#31350010). Medium was changed every day, and cells were splitted every other day using
407 TrypLE Express (Gibco; Cat #12605010) for harvesting. Cells were maintained in a 5% CO2
408 incubator at 37°C.

409 For inducing the ground-state of naïve pluripotency, mESCs were cultured in 2i/LIF medium
410 for 2 consecutive passages. 2i/LIF medium is composed by NDiff 227 medium (TAKARA, Cat
411 #Y40002) supplemented with 1000U/mL LIF, 0.4 µM PD032591 (Selleck Chemicals, Cat
412 #S1036) and 3 µM CHIR99021 (Merck, Cat #SML1046).

413 **Epiblast stem cell differentiation**

414 Differentiation from mESCs towards Epiblast Stem Cells (EpiSCs) was performed as previously
415 described [48]. $3x10^4$ mESCs were seeded in 6-well plastic dishes, and they were cultured in
416 Serum/LIF medium for 24h. Medium was then switched to NDiff 227 medium (TAKARA, Cat
417 #Y40002) supplemented with 20 ng/ml activin A (Cat. #120-14E; PeproTech) and 10 ng/ml Fgf
418 basic (R&D Systems, Cat #233-FB-025/CF). Cells were submitted to daily media changes till
419 day 5 (120h), when they were further analyzed.

420 **Embryoid bodies differentiation from mESCs**

421 Embryoid bodies differentiation was established as described in [49]. Briefly, mESCs were
422 splitted twice in Serum/LIF medium before inducing differentiation. Once mESCs are 80%
423 confluent, cells were collected using TrypLE Express. One well of 6-well plate was splitted in
424 an entire 6-well plate in IMDM-ES medium for 48h. IMDM-ES medium is composed of Iscove's
425 Modified Dulbecco's Medium (IMDM) (Cytiva, Cat #16SH30259.01) supplemented with 20%
426 FBS (ESC-qualified; Gibco Cat #26140079), 1X Glutamax (Gibco; Cat #35050061), 1X NEAA
427 (Gibco; Cat#11140050), 1mM Sodium Pyruvate (Gibco; Cat#11360070), 10ng/mL Leukemia
428 Inhibitory Factor (LIF) (Millipore, Cat #ESG1107) and 0.125mM 2-mercaptoethanol (Gibco;
429 Cat#31350010). For embryoid body induction, mESCs were harvested, and they were rinsed
430 twice with DPBS (Gibco; Cat #14190144). Cells were very well disaggregated into single-cells,
431 and 1.2 x 10^4 cells/mL embryoid body differentiation (EB^{diff}) medium were resuspended to a
432 total volume of 25mL of EB^{diff} medium. EB^{diff} medium is composed by IMDM supplemented
433 with 15% FBS (ESC-qualified; Gibco Cat #26140079), 1X Glutamax (Gibco; Cat #35050061), 50

434 µg/mL ascorbic acid (Sigma; Cat #A-4544), 180 µg/mL Transferrin (Roche; Cat #10652202001)
435 and 0.45 mM alpha-monothioglycerol (MTG) (Sigma; Cat #M6145). EBs were formed in
436 suspension for 5 days (120h). At day 5, in order to elongate the differentiation up to 216h
437 (day 9), EB^{diff} medium was refreshed by harvesting EBs with 10mL serological pipette,
438 centrifuge at 200 g for 3 min and EBs were resuspended in fresh EB^{diff} medium for 4 more
439 days.

440 **CRISPR/Cas9 gene editing and cell lines generation in mESCs**

441 The two guide RNAs (gRNAs) targeting the Nfkbia locus were designed using the CRISPR design
442 tool from MIT (http://crispr.mit.edu). The best 2 gRNAs (based on on-target and off-target
443 scores) that were targeting the exon 1 of Nfkbia (IκBα gene) were selected. After annealing,
444 one of the gRNAs was cloned into SpCas9(BB)-2A-GFP (px458) plasmid (Addgene; Cat #48138),
445 and the other gRNA was cloned into the px330-mCherry plasmid (modified from Addgene;
446 Cat #98750 to incorporate mCherry reporter). mESCs were co-transfected with the two
447 plasmids (px458-gRNA1 and px330-mCherry-gRNA2). $3x10^5$ cells were seeded a day before
448 per well of 6-well plate. At day of transfection, cells were washed once with 1X DPBS (Gibco;
449 Cat #14190144), and 2mL Opti-MEM medium (Gibco; Cat #31985070) was added into cells.
450 1.25 µg of each plasmid (2.5 µg of total DNA) was incubated with 10 µL of Lipofectamine 2000
451 (Invitrogen; Cat #11668019) in 240 µL of Opti-MEM for 20 min.
452 OptiMEM::Lipofectamine::DNA mixture was added into mESCs, and cells were incubated for
453 5 hours. Cells were then washed with DPBS, and medium was replaced by Serum/LIF. 48h
454 after transfection, GFP^+ $mCherry^+$ single cells were sorted by FACS using BD FACSAria II Cell
455 Sorter (BD Bioscience). Mutant clones were screened through PCR and western blotting to
456 identify single clones with no IκBα protein expression. Non-targeting scrambled gRNAs were
457 cloned into px458 and px330-mCherry plasmids as wildtype clones. Three independent clones
458 from each genotype (IκBα-WT and IκBα-KO) were selected for further experiments.

459 To increase IκBα specific detection, the IκBα endogenous gene (Nfkbia) was knocked-in with
460 3XFLAG sequence (DYKDHDGDYKDHDIDYKDDDDK) at the 3' end. To generate IκBα-3XFLAG
461 mESCs, 3XFLAG sequence was cloned into a plasmid containing Nfkbia left and right homology
462 arms flanking the endogenous stop codon; a spacer sequence of three glycines (GGCGGTGGG)
463 was also introduced to link the IκBα endogenous protein with the 3XFLAG (donor plasmid).
464 To induce the knock-in of the 3XFLAG, a gRNA complementary to the region surrounding the
465 endogenous stop codon was cloned into the PX458 plasmid (PX458-gRNA-mNfkbia-Cterm).
466 mESCs were co-transfected with donor and PX458-gRNA-mNfkbia-Cterm plasmids, cells were
467 sorted by FACS and individual clones were screened for IκBα-3XFLAG homozygous clones.
468 gRNAs and oligos sequences are included in supplementary table 1.

469 Doxycycline-inducible IκBα ($IκBα^{WT}$, $IκBα^{ΔNF-κB}$ and i-$IκBα^{ΔH2A/H4}$) mESCs were generated by
470 cloning the three different IκBα versions into a PiggyBac transposon system [50]. IκBα protein-
471 coding cDNAs were PCR-amplified, and NheI and SalI restriction sites were placed at the 5'

472 and 3' ends, respectively. T2A-EGFP fragment was amplified from PX458 plasmid, and SalI and
473 AgeI restriction sites were introduced at its 5' and 3' ends. PB-TRE backbone (Addgene, Cat#
474 63800) was digested with NheI and AgeI enzymes, and mNfkbia and T2A-EGFP fragments
475 were ligated into the PB-TRE digested vector. To generate mESCs containing the inducible
476 vector, IκBα-KO mESCs were co-transfected with PB-TRE-mNfkbia-T2A-EGFP and PiggyBac
477 transposase plasmids, and pool of transfected cells was selected by Hygromycin (100µg/mL)
478 for 7 days. Cells were doubly screened by FACS sorting green fluorescent protein after 24h of
479 doxycycline (1µg/mL) treatment. Pool of cells were used for further experiments. Oligos
480 sequences are included in supplementary table 1.

481 **Teratoma formation assay**

482 IκBα-WT and IκBα-KO mESCs grown in Serum/LIF (5×10^5) were injected intramuscularly into
483 severe combined immunodeficient mice (NSG). In order to favor 3D aggregation of cells and
484 teratoma formation, cells were resuspended in Matrigel Matrix (BD; Cat #356234) prior to
485 injection. Six weeks later, mice with tumors were euthanized, and tumors were fixed in
486 formaldehyde, embedded in paraffin, sectioned and stained with hematoxylin and eosin for
487 histological analysis.

488 **Immunofluorescence staining**

489 For immunostaining of mESCs, cells were seeded on 0.1% gelatin-coated coverslips on 6-well
490 plates; for EB immunofluorescence, they were collected directly from the plate. Samples were
491 washed twice with 1X PBS, and they were fixed at 4ºC for 30 minutes with 4% PFA (Electron
492 Microscopy Sciences; Cat #15713S). For immunofluorescence of 5-Methylcytosine (5mC),
493 fixed cells were incubated with 2M Hydrochloric Acid (Sigma-Aldrich, Cat #H1758) for 20
494 minutes at room temperature. Samples were then washed twice with 1X Tris-buffered saline
495 (TBS; 50 mM Tris-Cl, pH 8) and permeabilized and blocked with 1X TBS supplemented with 1%
496 Triton-X100 (MERCK; Cat #9036-19-5) and 6% FBS (Biological Industries; Cat #04-001-1A) for
497 2h at 4ºC. Samples were washed twice with 1X TBS supplemented with 6% FBS. Primary
498 antibody incubation was performed in 1X TBS plus 6% FBS and 0.3% or 0.5% Triton-X100 (0.3%
499 for 2D culture and 0.5% for EBs) overnight at 4ºC. The following primary antibodies were used:
500 OCT3/4 (1:250; Santa Cruz; Cat #sc-5279), NANOG (1:250; Novus Biologicals; Cat #NB100-
501 588), 5-Methylcytosine (1:500, Invitrogen, Cat #MA5-24694), H3K27Ac (1:2000, Abcam, Cat
502 #AB4729). Samples were then washed 4 times with 1X TBS, 5 min each washing. Secondary
503 antibody incubation was performed in TBS 1X plus 1% BSA (Sigma-Aldrich; Cat #9048-46-8)
504 for 2h at room temperature. The following antibodies were used: Alexa Fluor 488 donkey anti-
505 mouse antibody (1:1000; Invitrogen; Cat #A-21202), Alexa Fluor 647 donkey anti-mouse
506 antibody (1:1000; Invitrogen; Cat #A-31571), Alexa Fluor 594 donkey anti-rabbit antibody
507 (1:1000; Life Technologies; Cat #A-21207), Alexa Fluor 647 donkey anti-rabbit antibody
508 (1:1000, Invitrogen; Cat #A-31573). Samples were washed three times with 1X TBS for 5 min

509 at room temperature each rinse. Samples were mounted using DAPI Fluoromount-G
510 (Southern Biotech; Cat #0100-20).

511 **Microscopy and image acquisition**

512 Fluorescence images were acquired using Confocal Leica TCS SP5 (Leica Microsystems), and
513 Leica application software LAS AF (Leica Microsystems) was used to visualize the images.
514 Images of teratoma haematoxylin and eosin and immunohistochemistry stainings were
515 acquired using BX61 Olympus Microscope (Olympus), and PRECiV™ 2D Image and
516 Measurement Software (Olympus) was used to visualize the images. The Image J (version
517 1.15) was used for further analysis [51].

518 **Flow cytometry sample preparation and analysis**

519 Cells were collected and they were purified based on FACS using BD FACSAria II Cell Sorter
520 (BD Bioscience). Cells were sorted at 3,500 events/second, and at maximum flow rate of 4
521 and 85 µm nozzle. 5 µg/ml of DAPI (Biotium; Cat #BT-40043) was used as a viability dye. For
522 flow cytometry analysis of pluripotency exit, cells were disaggregated using TrypLE Express,
523 and they were incubated at 4ºC for 20 minutes with SSEA1-eFluor 660 Monoclonal Antibody
524 (1:200, Invitrogene, Cat #50-8813-42). BD LSRFortessa Cell Analyzer or BD LSR II Flow
525 Cytometer (BD Bioscience) were used for Flow Cytometry Analysis experiments. Flow
526 cytometry data were analyzed using FlowJo X v10.0.7 (BD Biosciences).

527 **RNA isolation, cDNA synthesis and quantitative RT-PCR**

528 Total RNA isolation from cells was performed using the RNeasy Plus Mini Kit (Qiagen; Cat
529 #74136) or RNeasy Micro Kit (Qiagen; Cat #74004) following manufacturer's instructions.
530 Amount of RNA was quantified with Nanodrop (Thermo Fisher; Cat #ND2000CLAPTOP), and
531 2 µg of total RNA was retro-transcribed using Transcriptor First Strand cDNA Synthesis Kit
532 (Roche; Cat #04897030001) following the manufacturer's instructions.

533 Quantitative RT-PCR was performed in triplicates for each sample, and SYBR Green I Master
534 Kit (Roche; Cat #04887352001) was used to carry out the reaction. qRT-PCR was performed
535 using the LightCycler 480 system (Roche). Relative expression levels were calculated as $2^{-\Delta CT}$
536 normalized with the average CT of the housekeeping gene Tbp or Gapdh. Oligos sequences
537 are found in supplementary table 1.

538 **Chromatin Immunoprecipitation (ChIP)**

539 4-6x10^7 mESCs were cross-linked by incubating them in DPBS (Gibco, Cat #14190094)
540 supplemented with 1% formaldehyde (Sigma-Aldrich; Cat #252549) for 10 min rocking at
541 room temperature. Cross-linking was stopped using 125 mM Glycine (Sigma-Aldrich, Cat
542 #G8790) rocking for 5 minutes at room temperature. Fixed cells were then washed twice with
543 ice-cold DPBS, and scrapped and collected using DPBS supplemented with

544 protease/phosphatase inhibitor cocktail composed by 1X cOmplete™, EDTA-free Protease
545 Inhibitor Cocktail (Roche, Cat #11873580001), 1 mM PMSF, 1mM Sodium Ortovanadate and
546 20 mM β-Glycerol phosphate. Cells were centrifuged at 3200g for 5 minutes at 4ºC. Cells were
547 lysed by resuspending cell pellet in ice-cold ChIP buffer (1 volume of SDS buffer [100mM NaCl,
548 50mM Tris-HCl pH 8.1, 5mM EDTA pH 8, 0.5% SDS] and 0.5 volume of triton dilution buffer
549 [100mM Tris-HCl pH 8.6, 100mM NaCl, 5mM EDTA pH 8, 5% Triton X-100]) supplemented with
550 protease/phosphatase inhibitor cocktail, and samples were sonicated using sonication beads
551 (Diagenode; Cat #C01020031) and the Bioruptor Pico Sonicator (Diagenode; Cat #B01060010)
552 for 20 cycles (each cycle 30 seconds on/30 seconds off) or till DNA fragments have 100-300bp
553 size. Samples were centrifuged at 16000g for 20 minutes at 4ºC. Chromatin was quantified,
554 and 30 µg of chromatin was incubated with every 5µg of antibody rotating for 16 hours (or
555 overnight) at 4ºC. The following antibodies were used: H3K4me3 (Abcam, Cat #ab8580),
556 H3K27me3 (Millipore, Cat ##07-449), H3K9me3 (Abcam, Cat #ab8898), H3K27Ac (Abcam, Cat
557 #ab4729), H3K4me1 (Abcam, Cat #ab8895). Samples were pulled down by incubation with
558 Protein A-Sepharose™ CL-4B (previously hydrated and blocked with 0.05% BSA) for 3h at 4ºC
559 in rotation. Sample was washed with a low salt washing buffer (50mM HEPES pH 7.5, 140mM
560 NaCl and 1% Triton) three times, one wash with a high salt wash buffer (50mM HEPES pH 7.5,
561 500mM NaCl and 1% Triton) and one wash with TE pH 8 (10mM Tris-HCl pH8, 1mM EDTA).
562 Samples were then eluted in 1% SDS and 100mM $NaHCO_3$. Samples were descrosslinked by
563 incubating for 16 hours (or overnight) at 65ºC shaking at 450 rpm, and were treated with
564 Proteinase K for 1h at 45ºC. DNA was purified using QIAquick PCR Purification Kit (Qiagen, Cat
565 #28106), following the manufacturer's instructions.

566 For ChIP IκBα-3XFLAG, a previous cross-linking step using Gold (Diagenode, Cat #C01019027)
567 was performed following manufacturer's instructions, and cells (IκBα$^{3XFLAG/3XFLAG}$ and IκBα-WT
568 mESCs) were later treated with 1% formaldehyde as mentioned above. Cell nuclei were
569 isolated by incubating cell pellets in a buffer containing 5mM Pipes pH 8, 85mM KCl and 0.5%
570 NP40, and later incubated on ice for 10 minutes followed by centrifuge at 4000 rpm for 5
571 minutes at 4ºC. Nucleus were lysed in a buffer containing 1% SDS, 10mM EDTA and 50 mM
572 Tris-HCl pH 8.1 and incubated on ice for 10 min. Samples were sonicated as mentioned above
573 and SDS was removed by incubating the sonicated sample on ice for 1 hour and later
574 centrifuged for 15 at 4ºC and 16000g. 60µg of chromatin was incubated with 10 µg of ANTI-
575 FLAG® M2 (Sigma-Aldrich, Cat #F1804). Samples were pulled down by a 50/50 mix of
576 Dynabeads A (Invitrogen, Cat #10002D) and G (Invitrogen, Cat #10003D). Samples were
577 washed 4 times in 0.1% SDS, 1% Triton-X, 2mM EDTA, 20mM Tris-HCl pH 8 and 150mM NaCl;
578 followed by 1 wash in TE pH 8.

579 For ChIP followed by PCR, 1 µL of ChIP sample was normalized by its input and enrichment
580 was calculated based on IgG isotype control. Oligos used are found in supplementary table 1.

581 For ChIP followed by sequencing (ChIP-seq) Purified DNA concentration and integrity were
582 determined using Agilent Bioanalyzer (Agilent Technologies; Cat #G2939BA). Libraries were

583 prepared using standard protocols. Chromatin was sequenced using Illumina HiSeq platform
584 (Illumina, Inc.) (50bp single-end reads). Samples sequencing depth range was the following:
585 (i) H3K4me3: 2.56-2.74x10^7 reads, (ii) H3K27me3: 6.19-7.2x10^7 reads, (iii) H3K9me3: 7.12-
586 8.92x10^7 reads, (iv) IκBα-3XFLAG: 9.81-10.86x10^7 reads, (v) H3K27Ac: 9.11-10.65x10^7 reads
587 and (vi) H3K4me1: 9.76-10.58x10^7 reads.

588 **ChIP-seq data analysis**

589 Quality control was performed on raw data with FASTQC tool. Raw reads were trimmed to
590 remove adapters presence with Trimgalore (v0.6.6) [52]. Default parameters were used except
591 for a minimum quality of 15 (Phred score) and an adapter removal stringency of 3bp overlap.
592 For H3K4me3, H3K27me3, H3K4me1 and IκBα-3XFLAG or IκBα-WT data, trimmed reads
593 were aligned to reference genome with Bowtie2 (v2.4.4) which was executed with default
594 parameters [53]. Required genome index was built with corresponding GRCm38 fasta file
595 retrieved from Ensembl (http://ftp.ensembl.org/pub/release-102/). Multimapped reads and
596 those exhibiting MAPQ < 20 were removed. For H3K9me3 data, trimmed reads were aligned
597 to reference genome (GRCm38 release 102 from Ensembl) with ShortStack (v3.8.5) [54].
598 Randomly placed multimappers were removed from the mapped reads. For all cases,
599 duplicated reads were marked with SAMtools (v1.15) [55]. Drosophila Melanogaster spike-ins,
600 present in H3K27me3, were discarded. NSC and RSC quality metrics were computed with
601 PhantomPeakQualTools (v1.2) [56]. ENCODE blacklisted regions (mm10 v2) were removed prior
602 to peak calling except for H3K9me3 (Amemiya et al., 2019). BigWig files were individually
603 generated using deepTools (v3.5.1) bamCoverage with -ignoreDuplicates -binSize 10 -
604 smoothLength 30 -effectiveGenomeSize 2308125349 -normalizeUsing RPGC and -
605 extendReads *Fragment_Length* options [57]. The effective genome size was particularized to a
606 read length of 50bp and directly retrieved from deepTools web site
607 (https://deeptools.readthedocs.io/en/develop/content/feature/effectiveGenomeSize.html).
608 *Fragment_Length* was retrieved from PhantomPeakQualTools results except for H3K9me3
609 where 150bp value was considered. Duplicates were kept in IκBα-3XFLAG for BigWig files
610 generation. For all histone marks except for H3K4me3, peak calling was conducted by means
611 of epic2 (v0.0.52) with -effective-genome-fraction 0.8452 -fragment-size *Fragment_Length*
612 options and chromosome sizes only referring to canonical chromosomes [58]. For H3K4me3 and
613 IκBα-3XFLAG/WT, MACS2 (v2.2.7.1) was used to identify peaks with -nomodel -extsize
614 *Fragment_Length* -g 2308125349 options [59]. The corresponding input sample was used in all
615 peak calling computations. For the histone marks, peaks were called with adjusted p-values
616 (FDR) < 0.05. In case of IκBα-3XFLAG/WT samples, peaks were called with adjusted p-values
617 (FDR) < 0.05 and a minimum 4-fold enrichment.

618 Peak annotation was performed with ChIPseeker R (v4.2.1) package (v1.34.1) considering a
619 TSS region range between 5000 bp upstream and 100 bp downstream (Yu et al., 2015).
620 Required TxDb object was generated from the Ensembl GRCm38 gtf file retrieved
621 (http://ftp.ensembl.org/pub/release-102/). A consensus peakset was obtained from the

622 three biological replicates per histone mark and condition (IκBα-WT or IκBα-KO) by identifying
623 overlapping peaks in at least two out of the three replicates. In case of IκBα ChIP-seq data,
624 peaks from consensus peakset identified from the -3XFLAG samples not overlapping with
625 IκBα-WT were considered the high-fidelity peaks for this experiment. For this purpose,
626 findOverlapsOfPeaks function from ChIPpeakAnno R package (v3.32.0) was used with default
627 parameters [60].

628 Differential binding analysis (DBA) was conducted with DiffBind (v3.8.4) per histone mark [61].
629 Default parameters were used except for the summits parameter which was set to 500bp for
630 all histone marks except for H3K4me3 (150bp) in order to consider, for testing, intervals of
631 1000bp or 300bp respectively. Summit values were selected to have interval widths between
632 the minimum and first quartile peak width values for each histone mark. EdgeR was the
633 statistical method used for all the three analyses. Differentially bound regions (DBRs)
634 between IκBα-KO and IκBα-WT samples were called with adjusted p-values (FDR) < 0.05.
635 Identified DBRs with any annotated gene were plotted with EnrichedHeatmap R package
636 (v1.18.1) [62]. To summarize replicates per condition, normalizeToMatrix function was used
637 based on corresponding BigWig files in w0 mean mode in 50bp windows. Tracks visualization
638 were obtained by means of Integrative Genomics Browser (IGV) tool [63].

639 **Enhancers activity identification**

640 Consensus peaksets derived from the three H3K27ac and H3K4me1 IκBα-WT mESCs replicates
641 were used to identify poised and active enhancers in an IκBα-WT scenario. Putative poised
642 enhancers were defined as those regions with H3K4me1 but no H3K27ac peaks. Putative
643 active enhancers were defined as those regions with H3K27ac and presence/absence
644 H3K4me1 peaks. To assess any differential enhancers activity in IκBα-KO vs IκBα-WT mESCs
645 cultured in Serum/LIF, differentially bound regions and consensus peaksets (IκBα-KO)
646 identified in H3K4me1 and H3K27ac were required. Putative gained or lost poised/active
647 enhancers in IκBα $^{-/-}$ were obtained with following criteria: (i) for gained/lost poised enhancers
648 in IκBα $^{-/-}$: a differential H3K4me1 increase/decrease and absence of H3K27ac peaks in IκBα $^{-/-}$
649 consensus peakset, (ii) for gained/lost active enhancers (without H3K4me1) in IκBα-KO: a
650 differential H3K27ac increase/decrease and absence of H3K4me1 in IκBα-KO consensus
651 peakset and (iii) for gained/lost active enhancers (with H3K4me1) in IκBα-KO: a differential
652 H3K27ac increase/decrease and presence of H3K4me1 in IκBα $^{-/-}$ consensus peakset.

653 A maximum gap of 1000bp was allowed for checking the overlap between two different
654 histone marks. For this purpose, the 'subsetByOverlaps' function from the IRanges R package
655 was used (v.2.34.1).

656 **Hi-C data visualization and TADs annotations**

657 Juicebox v1.9.8 was run locally to visualize Hi-C data from [42], specifically in the mESCs
658 (Serum/LIF) dataset. Corresponding maps from this dataset were already included in the tool.

659 To visualize contact maps, balanced normalization was considered and applied color range up
660 to 3 in the selected regions. Additionally, the list of 2,712 TADs with their corresponding
661 genome coordinates was retrieved and used to locate the identified IκBα binding peaks,
662 enhancers in the IκBα-WT scenario and showing differential activity together with
663 differentially expressed genes from in-house RNAseq data.

664 **RNA-seq experiments**

665 Total RNA from three independent clones from mESCs, 48h EBs and 96h EBs was isolated
666 using the RNeasy Plus Mini Kit (Qiagen; Cat #74136) following manufacturer's instructions.
667 Amount of RNA was quantified with Nanodrop (Thermo Fisher; Cat #ND2000CLAPTOP), and
668 RNA integrity was addressed by agarose gel and Agilent Bioanalyzer (Agilent Technologies;
669 Cat #G2939BA). Libraries sequenced using Illumina HiSeq 2500 (Illumina, Inc.) (125bp paired-
670 end reads). Samples sequencing depth ranged between 35M and 52M reads (average 41M
671 reads) per sample.

672 **RNA-seq data analysis**

673 Quality control was performed on raw data with the FASTQC tool (v0.11.9). Raw reads were
674 trimmed to remove adapter presence with Trimgalore (v0.6.6) [52]. Default parameters were
675 used except for a minimum quality of 15 (Phred score) and an adapter removal stringency of
676 3bp overlap. Trimmed reads were aligned to reference the genome with STAR aligner tool
677 (v2.7.8). STAR was executed with default parameters except for the number of allowed
678 mismatches which was set to 1. Required genome index was built with corresponding
679 GRCm38 gtf and fasta files retrieved from Ensembl (http://ftp.ensembl.org/pub/release-
680 102/). Obtained BAM files with uniquely mapped reads were considered for further analysis.
681 Raw gene expression was quantified using featureCounts tool from subRead software (v2.0.1)
682 with exon as feature [64]. The raw counts matrix was imported into the R Statistical Software
683 environment (v4.2.1) for downstream analysis. Raw expression matrix included 55,487 genes
684 per 18 samples in total. Experimental design considered three timepoints: mouse ESCs, EBs
685 at 48h and EBs at 96h. Each time point included 6 samples distributed in two conditions: 3
686 IκBα-WT and 3 IκBα-KO. Prior to statistical analysis, those genes with less than 10 raw counts
687 across the 6 samples under test were removed. After pre-filtering, 21,843 genes (mESCs),
688 21,424 genes (EBs 48h) or 21,664 genes (EBs 96h) were available for testing. For visualization
689 purposes, counts were normalized by the variance-stabilizing transformation method as
690 implemented in DESeq2 R package [65] (v1.38.3). Differential expression analysis (DEA) was
691 conducted with DESeq2. Each time point was independently analyzed. Fitted statistical model
692 included sample conditions as covariable with IκBα-WT as the reference. Obtained log2 fold
693 change values were shrunken with apeglm shrinkage estimator R package (v1.20.0) [66]. Raw p-
694 values were adjusted for multiple testing using the Benjamini-Hochberg False Discovery Rate
695 (FDR) [67]. Differentially Expressed Genes (DEGs) between IκBα-KO and IκBα-WT samples were

696 called with adjusted p-values (FDR) < 0.05 and absolute shrunken log2 Fold change > 1. Data
697 visualization was performed with the ggplot2 (v3.4.1).

698 **Genome-wide DNA methylation samples preparation**

699 DNA from frozen mESCs pellets was extracted using DNeasy Blood and Tissue Kit (Qiagen
700 GmbH, Hilden, Germany). Purified genomic DNA was quantified with Qubit (Invitrogen,
701 Carlsbad, CA, USA) according to manufacturer's instructions. Infinium Mouse Methylation
702 BeadChip (Illumina, Inc., San Diego, CA, USA) arrays were used to profile DNA methylation
703 genome wide. This platform allows over 285,000 methylation sites per sample to be
704 interrogated at single-nucleotide resolution. The samples were bisulfite converted using EZ
705 DNA Methylation-Gold™ Kit (Zymo Research, CA, USA) and were hybridized in the array
706 following the manufacturer's instructions.

707 **DNA methylation data analysis**

708 The DNA methylation profile of the studied samples was assessed using the Infinium Mouse
709 Methylation BeadChip Array (~285,000 methylation sites) as previously described [68]. Briefly,
710 raw signal intensities were obtained with GenomeStudio Software 2011.1 (Illumina) and DNA
711 methylation beta values were computed from raw IDAT files using GenomeStudio default
712 normalization with control probes and background subtraction. Quality control steps to
713 remove erratic probe signals were performed within the R statistical environment (v4.0.3).
714 We removed probes with detection p value > 0.01, genotyping probes and manufacturing
715 flagged (MFG) probes described in the Illumina manifest file
716 (https://support.illumina.com/downloads/infinium-mouse-methylation-manifest-file.html).
717 The differentially methylated probes (DMPs) between IκBα-WT and IκBα-KO samples were
718 computed separately for each time point (mESCs and EBs at 96h) by deriving a linear model
719 with the limma R package (v3.46.0). Each condition included 3 samples per time point. DMPs
720 with adjusted p-value (FDR) <0.05 and absolute mean methylation beta value difference
721 between conditions >0.3 were considered significant. DNA methylation analysis was
722 performed using the mm10 mouse genome reference build and the complete annotation was
723 downloaded from the annotated manifest file
724 (http://zwdzwd.github.io/InfiniumAnnotation#mouse) [38].

725 **Functional analysis**

726 Overrepresentation analysis was applied over lists of selected genes derived from RNA-seq
727 data (DEGs) or from ChIP-seq data (differentially bound regions). The Gene Ontology
728 (Biological Process ontology, GO BP terms), KEGG PATHWAY and WikiPathways databases for
729 Mus Musculus [69–71] were interrogated by means of clusterProfiler R package (v4.6.2) (Wu et
730 al., 2021). Corresponding Entrez identifiers were used. Benjamini-Hochberg procedure was
731 used to obtain adjusted p-values. Obtained GO BP terms were simplified using the simplify

732 function from clusterProfiler with default parameters. Overrepresented terms or processes
733 were called with adjusted p-values (FDR) < 0.05.

734 Gene Set Enrichment Analysis (GSEA) was performed for mESCs against the three cell states
735 signatures defined by other authors [72]. Briefly, each signature was composed of 200 genes
736 uniquely expressed in each state obtained from bulk RNA-seq performed per state. For this
737 purpose, the complete list of genes from mESCs samples (21,843 genes) was ranked based on
738 the shrunken log2 Fold Change obtained from DEA. GSEA was conducted through the
739 fgseaMultilevel function from fgsea R package (v1.24.0) [73] with default parameters.
740 Enrichment plots were generated with the same package.

741 Additionally, the testEnrichment function from SeSAMe R package (v1.14.2) [74] was used for
742 conducting functional analysis with default parameters over the list of DMPs. Probe design,
743 transcription factor binding site and histone modifications consensus database sets, included
744 in the same package, were interrogated.

745 Gene Set Variation Analysis (GSVA) R package (v1.46.0) with default parameters were used to
746 obtain Z-score values for genes annotated to endoderm (GO:0001706), mesoderm
747 (GO:0001707) and ectoderm (GO:0001705) GO BP terms [75].

Statistical analysis

Statistical analysis was performed with GraphPad Prism v.8.0.1. (GraphPad Software, Inc.). Unless specified, the comparison between two groups was performed with unpaired two-sided t-test. A p-value < 0.05 was considered significant.

DATA AVAILABILITY

All sequencing data is deposited at GEO under a SuperSeries with the accession number GSE239565)[https://www.ncbi.nlm.nih.gov/geo/query/acc.cgi?acc=GSE239565]. Individual SubSeries can be found at: GSE239563 (RNA-seq data), GSE239564 (ChIP-seq data) and GSE239562 (Methylation array data).

CODE AVAILABILITY

Scripts used to process the generated bulk RNA-seq and ChIP-seq data are available in Github repository: https://github.com/BigaSpinosaLab/IkBa_Naive_Pluripotency

ACKNOWLEDGEMENTS

We would like to acknowledge all members of the Bigas/Espinosa labs for helpful discussions. We are grateful for technical support to CRG/UPF Flow Cytometry Unit, CRG Genomics and Advanced Light Microscopy Units. This work has been supported by Spanish Ministry of Science and Innovation (PID2019-104695RB-I00, PLEC2021-007518, PDC2021-120817-I00), Generalitat de Catalunya (2021SGR 39) and Departament de Salut (SLT002/16/00299) to AB; the Spanish Ministry of Science and Innovation (PID2019-108322GB-100 and PID2022-142679NB-I00) to LDC; the Spanish Ministry of Science and Innovation (PID2021-123383NB-I00.) and the Agencia de Gestió d'Ajuts Universitaris i de Recerca (2021 SGR 01222) to BP. L.G.P has been a recipient of FI AGAUR fellowship (2019 FI-B 00151/2020 FI_B1 00130) from Generalitat de Catalunya. D.A-V was funded by the FIS fellowship (FI20/00130) from Instituto Carlos III. M.B. received funding from the Ramón Areces Foundation. M.M. is a recipient of a grant from the Instituto Carlos III, grant number CA22/00011 (co-funded by the European Social Fund Plus, ESF+ and by the European Union). A.V was a recipient of PI22-00548 funded by the Instituto de Salud Carlos III (ISCIII) and co-funded by the European Union.

AUTHOR CONTRIBUTION

L.G.P, L.E and A.B designed the study. L.G.P, D.A-V, M.B, A.I, J.G, J.B, D.A.E, C.A.G.P, C.B, V.R.C and A.V performed experiments. L.G.P, M.M, M.B and C.A.G.P performed bioinformatics analysis. L.G and A.B wrote the manuscript with input from all authors. C.B, A.V, A.V, P.M, L.D.C, G.S, B.P, M.E and L.E provided input on experimental design. L.E and A.B provided resources and supervised the research.

785 **FIGURE LEGENDS**

786 **Figure 1. IκBα specifically accumulates in the chromatin of the naïve pluripotent state. A.**
787 Schematic of pluripotent states in mouse embryonic stem cells (mESCs). mESCs were
788 maintained regularly in naïve pluripotency by culturing them in serum/LIF medium, or they
789 were polarized towards the ground state of naïve pluripotency by culturing them for two
790 passages in LIF plus Gsk3β (CHIR99021 or Chiron) and MEK (PD0325091) inhibitors (2i/LIF).
791 mESCs were further differentiated towards the primed pluripotent state (epiblast-like cells)
792 by culturing mESCs in a medium containing 20ng/mL Activin A and 10ng/mL Fgf2 for 120h. **B.**
793 **C.** Relative mRNA levels of the canonical IκB genes (*Nfkbia, Nfkbib, Nfkbie*) (**B**) or Nf-κB
794 effector genes (*Rela, c-Rel, Relb, Nfkb1, Nfkb2*) (**C**) across the different states of pluripotency.
795 Expression was normalized using the house-keeping gene *Tbp* relative to 2i/LIF. Data from
796 three independent experiments. Dots indicate mean values and error bars refer to ± standard
797 deviation (SD). **D.** Western blot analysis of IκBα protein distribution in cytoplasm,
798 nucleoplasm (Nucleus) or chromatin in cells at the ground-state of naïve pluripotency (2i/L),
799 naïve pluripotency (S/L) or primed pluripotency (Epi). **E.** Transcriptome and proteome
800 differences across naïve (2i/LIF) and primed (Epiblast-like cells or EpiSCs) pluripotent states.
801 Enriched transcripts and proteins in naïve state are highlighted in red (Log_2 fold-change < -1).
802 Enriched transcripts and proteins in the primed state are marked in dark gray (Log_2 fold-
803 change > 1). Data from [33]. **F.** Heatmap showing the expression levels of pluripotency (*Dppa4,*
804 *Pou5f1, Sox2, Prdm14, Klf4, Zfp42, Nanog*), differentiation (*Mesp1, Gata4, Gata6, Lhx1,*
805 *Wnt3a, Fgf5, Nes, Axin2, Wnt3, Eomes, Foxa2, T, Mixl1, Lef1*) and NF-κB (*Nfkbia, Nfkbib,*
806 *Nfkbie, Nfkbiz, Rela, c-Rel, Relb*) genes from the RNAseq samples at mESCs (Serum/LIF) and
807 differentiating cells (embryoid bodies) at 48h and 96h of IκBα-WT cells. . **G.** Schematic of the
808 approach followed to deplete IκBα protein in mESCs (upper panel) and western blot analysis
809 of three independent IκBα-WT and IκBα-KO mESC clones (bottom panel). **H.** Boxplots, violin
810 plots and individual values representing the normalized gene expression levels in IκBα-WT or
811 IκBα-KO mESCs, EBs 48h and EBs 96h. Considered genes are those annotated to NF-κB
812 signaling pathway (KEGG PATHWAY mmu04064). Box Plots: center line, median; lower and
813 upper hinges, first and third quartiles; whiskers, 1.5x interquartile range (IQR) extended to
814 the largest/smallest value within 1.5xIQR; no outliers present. Unpaired two-sided Wilcoxon
815 test applied.

816 **Figure 2. Lack of IκBα impairs the exit from naïve pluripotency. A.** PC1 and PC2 from Principal
817 Component Analysis (PCA) of normalized RNA-seq data from 3 different time points (mESCs,
818 48h EBs and 96h EBs) of IκBα-WT and IκBα-KO cells (three independent clones from each
819 genotype). **B.** Heatmap showing the expression levels of naïve pluripotency genes (*Gab1,*
820 *Sox2, Esrrb, Zfp42, Dppa4, Klf2, Prdm14, Klf4, Tfcp2l1*) from the RNAseq samples of IκBα-WT
821 and IκBα-KO EBs at 96h of **C, D, E**. Z-score values for gene sets referring to Endoderm (C),
822 Mesoderm (D) and Ectoderm (E) formation from The Gene Ontology database (GO:0001706,
823 GO:0001707 and GO:0001705 terms, respectively) and obtained from corresponding
824 expression levels at mESCs, 48h and 96h EBs IκBα-WT or IκBα-KO cells (three independent

825 clones of each genotype). Loess curves are also represented with 95% confidence intervals.
826 **F.** Representative immunofluorescence of 216h EBs stained with the pluripotency markers
827 NANOG and OCT3/4. **G.** Quantification of total number of alkaline phosphatase (AP) colonies
828 after 216h EB differentiation and additional culture of 96h in Serum/LIF (S/L) medium. Dots
829 represent values from two independent experiments from three different IκBα-WT or IκBα-
830 KO clones. Unpaired two-sided t-test applied. **H.** Schematics of mESCs differentiation towards
831 Epiblast Stem Cells (EpiSCs). mESCs cultured in Serum/LIF were then seeded in N2B27 medium
832 supplemented with 10ng/mL Fgf2 and 20ng/mL Activin A for 120h (see Materials and
833 Methods section for further information). **I.** Relative RNA levels of naïve pluripotency genes
834 (*Dppa3, Nanog, Sox2, Rex1, Klf2, Klf4, Gbx2, Tbx3*) in IκBα-WT or IκBα-KO EpiSCs at 120h. RNA
835 levels were normalized based on *Tbp* expression relative to IκBα-WT. Each dot represents an
836 independent clone either from IκBα-WT or IκBα-KO genotypes. Unpaired two-sided t-test
837 applied. Horizontal bars indicate mean values and error bars refer to ± SD.

838 **Figure 3. IκBα-KO mESCs preserve the ground-state of naïve pluripotency under Serum/LIF**
839 **culture. A.** GSEA results comparing IκBα-KO vs IκBα-WT mESCs cultured in Serum/LIF against
840 ground (2i/LIF) and naïve (Serum/LIF) state pluripotency signatures retrieved from [36].
841 Adjusted p-value by Benjamini-Hochberg procedure and Normalized Enrichment Score (NES)
842 indicated. **B.** Heatmap showing the expression levels of the naïve pluripotency genes from
843 the RNAseq samples of IκBα-KO and IκBα-WT mESCs cultured in Serum/LIF. **C.** Number of
844 differentially bound regions (adjusted p-value <0.05, FDR) for H3K4me3, H3K27me3 and
845 H3K9me3 histone marks in IκBα $^{-/-}$ vs IκBα $^{+/+}$ mESCs cultured in Serum/LIF. Enriched or
846 reduced regions in IκBα $^{-/-}$ mESCs are distinguished (log_2 Fold-change >0 or <0, respectively).
847 Overrepresented WikiPathways, for (left) H3K4me3 and (center) H3K27me3, or The Gene
848 Ontology terms, for (right) H3K9me3 (adjusted p-value < 0.05, FDR) are indicated per mark.
849 Annotated genes to differential regions showing H3K4me3 enrichment, H3K27me3 reduction
850 or H3K9me3 reduction in IκBα-KOmESCs were considered. A one-sided hypergeometric test
851 was conducted. **D.** Representative naïve pluripotency genes having differential H3K4me3
852 (enriched) and H3K27me3 (reduced) levels in IκBα $^{-/-}$ vs IκBα $^{+/+}$ mESCs cultured in Serum/LIF.
853 Shadowed regions highlight the differential levels of the histone marks. **E.** Representative
854 immunofluorescence images of DNA-methylation-related mark 5-methylcytosine (5mC) in
855 IκBα-WT (left) and IκBα-KO (right) mESCs cultured in Serum/LIF. **F.** DNA methylation profile in
856 IκBα-WT vs IκBα-KO mESCs (left) and 96h EBs (right) showing the distribution density of mean
857 ß-values from all 261,220 CpGs under test per condition. **G.** DNA methylation levels in
858 different genomic regions in either IκBα-WT vs IκBα-KO mESCs or 96h EBs: promoters, gene
859 bodies, enhancers and imprinted regions. Number of CpGs analyzed in each category is
860 indicated between brackets. Unpaired two-sided t-test was applied.

861 **Figure 4. IκBα binds to enhancer regions to prevent their hyperactivation in the naïve**
862 **pluripotency state. A.** Distribution of genomic regions annotated to the 817 identified IκBα
863 chromatin binding peaks. **B, C.** H3K27Ac (B) and H3K4me1 (C) distribution profiles in IκBα-WT
864 vs IκBα-KO mESCs cultured in Serum/LIF across IκBα-bound chromatin regions. Histone marks

865 data generated in this study. **D.** Number of regions with differential enhancer activity in IκBα-
866 KO vs IκBα-WT mESCs cultured in Serum/LIF. Increased/Reduced activity for (left) poised
867 enhancers based on the H3K4me1 differential binding and absence of H3K27ac overlapping
868 peaks in IκBα-KO mESCs and, (right) active enhancers based on the differential binding of
869 H3K27ac and presence of H3K4me1 overlapping peaks in IκBα-KO. Differential binding based
870 on adjusted p-value <0.05 (FDR). Increased or reduced regions in IκBα-KO are distinguished
871 by $\log_2$ Fold-change >0 or <0, respectively, compared to IκBα-WT mESCs. Overrepresented
872 WikiPathways for annotated genes to (left) poised enhancers with reduced activity and (right)
873 active enhancers with increased activity in IκBα-KO vs IκBα-WT mESCs are indicated
874 (adjusted p-value < 0.05, FDR). A one-sided hypergeometric test was conducted. **E.**
875 Representative naïve pluripotency genes having an increase in active enhancer status
876 (H3K27Ac enrichment without changes in H3K4me1) in IκBα-KO mESCs cultured in Serum/LIF.
877 Shadowed regions highlight the differential levels of the histone mark. **F.** Heatmap showing
878 the expression levels of selected naïve pluripotency genes contained in TADs with active
879 enhancer marks (H3K27Ac and H3K4me1) and IκBα chromatin binding from RNAseq samples
880 of IκBα-WT and IκBα-KO mESCs and 48h EBs. **G.** (Upper panel) Contact map (Hi-C data from
881 [42]) of the TAD (chr5:118,785,000-119,707,000) which contains the Tbx3 locus. An extended
882 region is shown (chr5:118660246-119843912). Arrows indicate the interaction between the
883 IκBα-bound region and TSS of Tbx3 gene (upper arrow) or differential active enhancer
884 (bottom arrow). (Center panel) Genome browser showing ChIP-seq data from H3K27Ac and
885 H3K4me1 in IκBα-WT and IκBα-KO mESCs, and identified IκBα chromatin peaks. Shadowed
886 areas indicate differential active enhancer (light gray), the TSS of the gene of interest (darker
887 gray) or IκBα peaks (dark green). (Bottom panel) *Tbx3* expression (RNA-seq data) in IκBα-WT
888 and IκBα-KO mESCs and 48h EBs from two independent clones of each genotype. **H.**
889 Schematic representation of IκBα reconstitution of IκBα-KO mESCs. IκBα-KO mESCs were
890 reconstituted by introducing a doxycycline-inducible IκBα construct (i-IκBα^{WT}). mESCs were
891 then kept in Serum/LIF medium supplemented with 1µg/mL Doxycycline for 4 consecutive
892 passages. **I.** Western blot analysis of H3K27Ac levels in i-IκBα^{WT} mESCs (left panel). Two
893 independent experiments were performed to quantify H3K27Ac levels (right panel).

894 **Figure 5. IκBα safeguards enhancer hyperactivation in naïve pluripotency in an NF-κB-**
895 **independent manner. A.** Schematic of chromatin-specific/NF-κB-deficient (IκBα$^{\Delta NF\text{-}\kappa B}$) or NF-
896 κB-specific/chromatin-deficient (IκBα$^{\Delta Chrom}$) IκBα mutants (Separation-Of-Function or SOF
897 mutants). **B.** Pull-down of GST-H2A with cell lysates from different SOF IκBα mutant mESCs.
898 **C.** Pull-down of GST-p50 with lysates from SOF IκBα mutant mESCs. **D.** Western blot analysis
899 of chromatin protein extracts of doxycycline-inducible IκBα forms (i-IκBα$^{\Delta WT}$, i-IκBα$^{\Delta NF\text{-}\kappa B}$,
900 IκBα$^{\Delta Chrom}$) after 16h of doxycycline induction. **E.** Western blot analysis of H3K27Ac levels in i-
901 IκBα^{WT}, i-IκBα$^{\Delta NF\text{-}\kappa B}$ and IκBα$^{\Delta Chrom}$ mESCs (upper panel). H3K27Ac levels were quantified
902 (bottom panel). **F, G.** ChIP followed by PCR of H3K27Ac (F) and H3K4me1 (G) marks within
903 genomic regions bound by IκBα in i-IκBα$^{\Delta NF\text{-}\kappa B}$ and IκBα$^{\Delta Chrom}$ mESCs cultured in Serum/LIF.
904 Unpaired two-sided t-test was performed. Bars indicate mean values and error bars refer to

905 ± standard error of the mean (SEM). **H.** Representative immunofluorescence images of DNA-
906 methylation-related mark 5-methylcytosine (5mC) in i-IκBα$^{\Delta WT}$ (upper panel), i-IκBα$^{\Delta NF\text{-}\kappa B}$
907 (medium panel), IκBα$^{\Delta Chrom}$ (bottom panel) mESCs cultured in Serum/LIF. **I.** Flow cytometry
908 analysis of the pluripotency surface marker SSEA-1 at 216h EBs in i-IκBα^{WT}, i-IκBα$^{\Delta NF\text{-}\kappa B}$ and i-
909 IκBα$^{\Delta Chrom}$ cells. **J.** Quantification of Alkaline Phosphatase (AP) staining in 216h EBs upon
910 reconstitution with the different IκBα forms. Each dot represents an independent experiment.
911 One-way ANOVA was applied. Bars indicate mean values and error bars refer to ± SEM. **K.**
912 Representative immunofluorescence for NANOG and OCT3/4 at 216h EBs in i-IκBα^{WT} (upper
913 panel), i-IκBα$^{\Delta NF\text{-}\kappa B}$ (medium panel) and i-IκBα$^{\Delta Chrom}$ (bottom panel) cells.

914 **Figure 6. Proposed model: IκBα attenuates enhancer activity in the naïve-to-primed**
915 **pluripotency transition.** In mESCs cultured in Serum/LIF, IκBα binds to distal regions to
916 maintain a moderate pluripotency gene expression by avoiding enhancer hyperactivation.
917 This allows naïve pluripotency exit and differentiation upon LIF withdrawal. In the absence of
918 IκBα, enhancer regions acquire a higher activation status, resulting in an aberrantly increased
919 expression of pluripotency genes. This leads to an impaired pluripotency exit and
920 differentiation.

921 **Figure S1. Depletion of IκBα in mESCs compromises the exit from naïve pluripotency.**
922 **Related to Figure 2. A.** Volcano plot from differential expression analysis between IκBα-KO vs
923 IκBα-WT 96h EBs. Dashed vertical lines represent an absolute shrunken $\log_2$ Fold Change = 1
924 and dashed horizontal line represents an adjusted p-value = 0.05 (FDR). **B.** Boxplots and
925 individual values showing the quantification of relative size of 168h EBs. Each dot represents
926 an embryoid body. Unpaired two-sided t-test was applied. **C.** Relative RNA levels of naïve
927 pluripotency genes (*Pou5f1, Gbx2, Klf2, Sox2, Rex1, Nanog*) in IκBα-WT or IκBα-KO 216h EBs.
928 RNA levels were normalized based on *Tbp* expression relative to IκBα-WT . Each dot
929 represents an independent clone either from IκBα-WT or IκBα-KO genotypes. Unpaired two-
930 sided t-test was applied. **D.** Schematic of Alkaline Phosphatase (AP) staining carried out in EBs.
931 IκBα-WT or IκBα-KO 216h EBs were dissociated and seeded in Serum/LIF medium for another
932 96h. Attached cells were screened for AP^+ total cell number. **E.** Flow cytometry plots of SSEA-
933 1 from IκBα-WT or IκBα-KO EBs 216h. **F.** Schematic of teratoma formation assay. $5x10^5$ IκBα-
934 WT or IκBα-KO mESCs cultured in Serum/LIF were injected intramuscularly in the leg of
935 immunocompromised NSG mice. 6 weeks after the transplant, teratomas were formed, and
936 mice were euthanized for further teratoma analysis. **G.** Representative images of
937 immunohistochemistry for OCT3/4 in IκBα-WT (left panel) or IκBα-KO (right panel) teratomas.
938 Teratomas were derived from three independent clones of mESCs of both genotypes. **H.**
939 Percentage of OCT3/4+ cells in teratomas. Positive cells were counted from five different
940 microscope fields from each IκBα-WT and IκBα-KO clone. Unpaired two-sided t-test was
941 performed. Bars indicate mean values and error bars refer to ± SD. **I.** Brightfield images of
942 IκBα-WT or IκBα-KO EpiSCs at 120h. Each picture corresponds to an independent clone from
943 either IκBα-WT or IκBα-KO genotypes.

Figure S2. Absence of IκBα favors the ground-state of naïve pluripotency in Serum/LIF conditions. Related to Figure 3. A. Relative RNA levels of the naïve pluripotency genes *Rex1 (Zfp42), Klf2* and *Tbx3* upon culture of IκBα-WT either in Serum/LIF or two passages in 2i/LIF. 2i/LIF IκBα-WT mESCs were compared with IκBα-KO mESCs cultured in Serum/LIF. Unpaired two-sided t-test was applied to calculate statistical significance. Each dot represents an independent clone from each of the two genotypes. **B, C, D.** Volcano plots from differential binding analysis of H3K4me3 (B), H3K27me3 (C) and H3K9me3 (D) in IκBα-WT vs IκBα-KO mESCs cultured in Serum/LIF. Representative genes with enriched or reduced levels of H3K4me3 (B), H3K27me3 (C) and H3K9me3 (D) marks in IκBα-KO mESCs are highlighted. **E, F.** DNA methylation levels (mean ß-values) across chromosomes in IκBα-WT vs IκBα-KO mESCs (E) or 96h EBs (F).

Figure S3. IκBα binds to enhancer regions to preserve their proper activation level. Related to Figure 4. A. Heatmap of the chromatin binding profile of IκBα in mESCs cultured in Serum/LIF. High-fidelity IκBα chromatin peaks (n=817) were retrieved by considering common peaks in at least two out of the three different replicates in IκBα$^{3XFLAG/3XFLAG}$ mESCs that were not identified in IκBα-WT mESCs. ChIP of 3XFLAG was performed in either of the two conditions (IκBα$^{3XFLAG/3XFLAG}$ or IκBα-WT mESCs). **B, C .** H3K27Ac (B) or H3K4me1 (C) distribution profile in naïve (Serum/LIF) or primed (EpiSCs) pluripotency state across IκBα-bound chromatin regions. Histone marks data retrieved from [76]**. D.** Western blot analysis of H3K27Ac (Active enhancer) and H3K4me1 (total enhancer) in IκBα-WT vs IκBα-KO mESCs cultured in Serum/LIF. Two independent IκBα-KO mESC clones were analyzed. **E.** Representative immunofluorescence images of H3K27Ac in mESCs cultured in Serum/LIF. **F, G.** Volcano plots from differential binding analysis of H3K4me1 (F) and H3K27Ac (G) in IκBα-WT vs IκBα-KO mESCs cultured in Serum/LIF. Representative genes annotated to regions with enriched or reduced levels of histones marks in IκBα-KO mESCs are highlighted. **H.** Distribution of Topologically Associated Domains (TADs) into A (active) and B (inactive) compartments in a genome-wide fashion (left) or only for those including at least one IκBα peaks (right). Respective proportion of differential enhancers (poised or active as defined in panel B) are shown. Among the 74% of genome-wide TADs with differential enhancers, 69% of them were located within A compartment. Among the 92% of TADs with IκBα peak with differential enhancers, 81% of them were located within A compartment. TADs were retrieved from [42], mESCs dataset. **I.** Representative immunofluorescence images of H3K27Ac in i-IκBα^{WT} (bottom panel) mESCs vs IκBα-KO mESCs (upper panel) cultured in Serum/LIF. **J.** Relative RNA levels of naïve pluripotency genes (*Zfp42, Klf2, Sox2, Tbx3*) in i-IκBα^{WT} mESCs after doxycycline induction. Relative RNA levels were calculated based on *Tbp* expression. Each dot represents an independent experiment. Unpaired two-sided t-test was performed. Bars indicate mean values and error bars refer to ± SD.

Figure S4. Generation of separation-of-function (SOF) IκBα mutants demonstrates that IκBα safeguards hyperactivation of enhancers in an NF-κB-independent manner. Related to Figure 5. A. Relative expression level of Nfkbia gene after overnight doxycycline induction in

984 i-IκBα$^{\Delta WT}$, i-IκBα$^{\Delta NF\text{-}\kappa B}$ and IκBα$^{\Delta Chrom}$ mESCs. **B.** Western blot analysis of cytoplasmic protein
985 extracts of doxycycline-inducible IκBα forms (i-IκBα$^{\Delta WT}$, i-IκBα$^{\Delta NF\text{-}\kappa B}$, i-IκBα$^{\Delta Chrom}$) after 16h of
986 doxycycline induction. **C.** Schematic representation of reconstitution of IκBα-KO mESCs with
987 either of the two doxycycline-inducible SOF mutants (i-IκBα$^{\Delta NF\text{-}\kappa B}$ or IκBα$^{\Delta Chrom}$). mESCs were
988 then kept in Serum/LIF medium supplemented with 1μg/mL Doxycycline for 4 consecutive
989 passages. mESCs were characterized at the epigenetic level and then their potential to be
990 further differentiated was addressed. **D.** Representative immunofluorescence images of
991 H3K27Ac in i-IκBα$^{\Delta NF\text{-}\kappa B}$ (upper panel) mESCs vs i-IκBα$^{\Delta Chrom}$ mESCs (bottom panel) cultured in
992 Serum/LIF**. E.** Relative RNA levels of naïve pluripotency genes (*Zfp42, Klf2, Sox2, Tbx3*) in i-
993 IκBα$^{\Delta NF\text{-}\kappa B}$ and i-IκBα$^{\Delta Chrom}$ mESCs after doxycycline induction. Unpaired two-sided t-test was
994 performed.Bars indicate mean values and error bars refer to +/- standard deviation. **F.**
995 Percentage of differentiated cells (determined as SSEA-1.) at 216h EBs 216h derived from i-
996 IκBα$^{\Delta WT}$, i-IκBα$^{\Delta NF\text{-}\kappa B}$ and IκBα$^{\Delta Chrom}$ mESCs. **G.** Representative images of Alkaline Phosphatase
997 (AP) staining in 216h EBs upon reconstitution with the different IκBα forms. **H.** Quantification
998 of EB differentiation status (percentage of pluripotent cells) at 216h after induction of SOF
999 IκBα mutants. Data from two independent experiments.

1000 **REFERENCES**

1001 1. Festuccia, N., Osorno, R., Wilson, V., and Chambers, I. (2013). The role of pluripotency
1002 gene regulatory network components in mediating transitions between pluripotent cell
1003 states. Curr. Opin. Genet. Dev. *23*, 504–511.

1004 2. Graf, T., and Stadtfeld, M. (2008). Heterogeneity of embryonic and adult stem cells. Cell
1005 Stem Cell *3*, 480–483.

1006 3. Martinez Arias, A., and Brickman, J.M. (2011). Gene expression heterogeneities in
1007 embryonic stem cell populations: origin and function. Curr. Opin. Cell Biol. *23*, 650–656.

1008 4. Pera, M.F., and Rossant, J. (2021). The exploration of pluripotency space: Charting cell
1009 state transitions in peri-implantation development. Cell Stem Cell *28*, 1896–1906.

1010 5. Wang, X., and Wu, Q. (2022). The Divergent Pluripotent States in Mouse and Human
1011 Cells. Genes *13*. 10.3390/genes13081459.

1012 6. Ying, Q.-L., Wray, J., Nichols, J., Batlle-Morera, L., Doble, B., Woodgett, J., Cohen, P.,
1013 and Smith, A. (2008). The ground state of embryonic stem cell self-renewal. Nature
1014 *453*, 519–523.

1015 7. Marks, H., Kalkan, T., Menafra, R., Denissov, S., Jones, K., Hofemeister, H., Nichols, J.,
1016 Kranz, A., Stewart, A.F., Smith, A., et al. (2012). The transcriptional and epigenomic
1017 foundations of ground state pluripotency. Cell *149*, 590–604.

1018 8. Boroviak, T., Loos, R., Lombard, P., Okahara, J., Behr, R., Sasaki, E., Nichols, J., Smith, A.,
1019 and Bertone, P. (2015). Lineage-Specific Profiling Delineates the Emergence and
1020 Progression of Naive Pluripotency in Mammalian Embryogenesis. Dev. Cell *35*, 366–
1021 382.

1022 9. Brons, I.G.M., Smithers, L.E., Trotter, M.W.B., Rugg-Gunn, P., Sun, B., Chuva de Sousa
1023 Lopes, S.M., Howlett, S.K., Clarkson, A., Ahrlund-Richter, L., Pedersen, R.A., et al.
1024 (2007). Derivation of pluripotent epiblast stem cells from mammalian embryos. Nature
1025 *448*, 191–195.

1026 10. Tesar, P.J., Chenoweth, J.G., Brook, F.A., Davies, T.J., Evans, E.P., Mack, D.L., Gardner,
1027 R.L., and McKay, R.D.G. (2007). New cell lines from mouse epiblast share defining
1028 features with human embryonic stem cells. Nature *448*, 196–199.

1029 11. Weinberger, L., Ayyash, M., Novershtern, N., and Hanna, J.H. (2016). Dynamic stem cell
1030 states: naive to primed pluripotency in rodents and humans. Nat. Rev. Mol. Cell Biol.
1031 *17*, 155–169.

1032 12. Guo, G., Yang, J., Nichols, J., Hall, J.S., Eyres, I., Mansfield, W., and Smith, A. (2009). Klf4
1033 reverts developmentally programmed restriction of ground state pluripotency.
1034 Development *136*, 1063–1069.

1035 13. Takahashi, S., Kobayashi, S., and Hiratani, I. (2018). Epigenetic differences between

1036 naïve and primed pluripotent stem cells. Cell. Mol. Life Sci. *75*, 1191–1203.

1037 14. Bao, S., Tang, F., Li, X., Hayashi, K., Gillich, A., Lao, K., and Surani, M.A. (2009).
1038 Epigenetic reversion of post-implantation epiblast to pluripotent embryonic stem cells.
1039 Nature *461*, 1292–1295.

1040 15. Habibi, E., Brinkman, A.B., Arand, J., Kroeze, L.I., Kerstens, H.H.D., Matarese, F.,
1041 Lepikhov, K., Gut, M., Brun-Heath, I., Hubner, N.C., et al. (2013). Whole-genome
1042 bisulfite sequencing of two distinct interconvertible DNA methylomes of mouse
1043 embryonic stem cells. Cell Stem Cell *13*, 360–369.

1044 16. Leitch, H.G., McEwen, K.R., Turp, A., Encheva, V., Carroll, T., Grabole, N., Mansfield, W.,
1045 Nashun, B., Knezovich, J.G., Smith, A., et al. (2013). Naive pluripotency is associated
1046 with global DNA hypomethylation. Nat. Struct. Mol. Biol. *20*, 311–316.

1047 17. Singer, Z.S., Yong, J., Tischler, J., Hackett, J.A., Altinok, A., Surani, M.A., Cai, L., and
1048 Elowitz, M.B. (2014). Dynamic heterogeneity and DNA methylation in embryonic stem
1049 cells. Mol. Cell *55*, 319–331.

1050 18. Factor, D.C., Corradin, O., Zentner, G.E., Saiakhova, A., Song, L., Chenoweth, J.G.,
1051 McKay, R.D., Crawford, G.E., Scacheri, P.C., and Tesar, P.J. (2014). Epigenomic
1052 comparison reveals activation of "seed" enhancers during transition from naive to
1053 primed pluripotency. Cell Stem Cell *14*, 854–863.

1054 19. Buecker, C., Srinivasan, R., Wu, Z., Calo, E., Acampora, D., Faial, T., Simeone, A., Tan,
1055 M., Swigut, T., and Wysocka, J. (2014). Reorganization of enhancer patterns in
1056 transition from naive to primed pluripotency. Cell Stem Cell *14*, 838–853.

1057 20. Zhang, Q., Lenardo, M.J., and Baltimore, D. (2017). 30 Years of NF-κB: A Blossoming of
1058 Relevance to Human Pathobiology. Cell *168*, 37–57.

1059 21. Aguilera, C., Hoya-Arias, R., Haegeman, G., Espinosa, L., and Bigas, A. (2004).
1060 Recruitment of IκBα to the *hes1* promoter is associated with transcriptional repression.
1061 Proceedings of the National Academy of Sciences *101*, 16537–16542.

1062 22. Mulero, M.C., Ferres-Marco, D., Islam, A., Margalef, P., Pecoraro, M., Toll, A., Drechsel,
1063 N., Charneco, C., Davis, S., Bellora, N., et al. (2013). Chromatin-bound IκBα regulates a
1064 subset of polycomb target genes in differentiation and cancer. Cancer Cell *24*, 151–166.

1065 23. Marruecos, L., Bertran, J., Álvarez-Villanueva, D., Mulero, M.C., Guillén, Y., Palma, L.G.,
1066 Floor, M., Vert, A., Arce-Gallego, S., Pecharroman, I., et al. (2021). Dynamic chromatin
1067 association of IκBα is regulated by acetylation and cleavage of histone H4. EMBO Rep.
1068 *22*, e52649.

1069 24. Marruecos, L., Bertran, J., Guillén, Y., González, J., Batlle, R., López-Arribillaga, E.,
1070 Garrido, M., Ruiz-Herguido, C., Lisiero, D., González-Farré, M., et al. (2020). IκBα
1071 deficiency imposes a fetal phenotype to intestinal stem cells. EMBO Rep. *21*, e49708.

1072 25. Thambyrajah, R., Fadlullah, Z., Proffitt, M., Neo, W.H., Guillén, Y., Casado-Pelaez, M.,

1073 Herrero-Molinero, P., Brujas, C., Castelluccio, N., González, J., et al. (2022). IκBα
1074 controls dormancy induction in Hematopoietic stem cell development via retinoic acid.
1075 bioRxiv, 2022.11.17.516971. 10.1101/2022.11.17.516971.

1076 26. Gerondakis, S., Grumont, R., Gugasyan, R., Wong, L., Isomura, I., Ho, W., and Banerjee,
1077 A. (2006). Unravelling the complexities of the NF-kappaB signalling pathway using
1078 mouse knockout and transgenic models. Oncogene *25*, 6781–6799.

1079 27. Kaltschmidt, C., Greiner, J.F.W., and Kaltschmidt, B. (2021). The Transcription Factor
1080 NF-κB in Stem Cells and Development. Cells *10*. 10.3390/cells10082042.

1081 28. Li, S., Sun, J., Zhang, B.-W., Yang, L., Wan, Y.-C., Chen, B.-B., Xu, N., Xu, Q.-R., Fan, J.,
1082 Shang, J.-N., et al. (2024). ATG5 attenuates inflammatory signaling in mouse embryonic
1083 stem cells to control differentiation. Dev. Cell. 10.1016/j.devcel.2024.01.026.

1084 29. Torres, J., and Watt, F.M. (2008). Nanog maintains pluripotency of mouse embryonic
1085 stem cells by inhibiting NFkappaB and cooperating with Stat3. Nat. Cell Biol. *10*, 194–
1086 201.

1087 30. Dutta, D., Ray, S., Home, P., Larson, M., Wolfe, M.W., and Paul, S. (2011). Self-renewal
1088 versus lineage commitment of embryonic stem cells: protein kinase C signaling shifts
1089 the balance. Stem Cells *29*, 618–628.

1090 31. Espín-Palazón, R., and Traver, D. (2016). The NF-κB family: Key players during
1091 embryonic development and HSC emergence. Exp. Hematol. *44*, 519–527.

1092 32. Alvarez-Villanueva, D., Galan, L., Bertran, J., and Floor, M. (2023). Separation-of-
1093 function mutants reveal the NF-κB-independent involvement of IκBα in the regulation
1094 of stem cell and oncogenic programs. bioRxiv.

1095 33. Atlasi, Y., Jafarnejad, S.M., Gkogkas, C.G., Vermeulen, M., Sonenberg, N., and
1096 Stunnenberg, H.G. (2020). The translational landscape of ground state pluripotency.
1097 Nat. Commun. *11*, 1617.

1098 34. Hayden, M.S., and Ghosh, S. (2008). Shared principles in NF-kappaB signaling. Cell *132*,
1099 344–362.

1100 35. Basak, S., Kim, H., Kearns, J.D., Tergaonkar, V., O'Dea, E., Werner, S.L., Benedict, C.A.,
1101 Ware, C.F., Ghosh, G., Verma, I.M., et al. (2007). A fourth IkappaB protein within the
1102 NF-kappaB signaling module. Cell *128*, 369–381.

1103 36. Ghimire, S., Van der Jeught, M., Neupane, J., Roost, M.S., Anckaert, J., Popovic, M., Van
1104 Nieuwerburgh, F., Mestdagh, P., Vandesompele, J., Deforce, D., et al. (2018).
1105 Comparative analysis of naive, primed and ground state pluripotency in mouse
1106 embryonic stem cells originating from the same genetic background. Sci. Rep. *8*, 5884.

1107 37. Yagi, M., Kishigami, S., Tanaka, A., Semi, K., Mizutani, E., Wakayama, S., Wakayama, T.,
1108 Yamamoto, T., and Yamada, Y. (2017). Derivation of ground-state female ES cells
1109 maintaining gamete-derived DNA methylation. Nature *548*, 224–227.

1110 38. Zhou, W., Hinoue, T., Barnes, B., Mitchell, O., Iqbal, W., Lee, S.M., Foy, K.K., Lee, K.-H.,
1111 Moyer, E.J., VanderArk, A., et al. (2022). DNA methylation dynamics and dysregulation
1112 delineated by high-throughput profiling in the mouse. Cell Genom *2*.
1113 10.1016/j.xgen.2022.100144.

1114 39. Choi, J., Huebner, A.J., Clement, K., Walsh, R.M., Savol, A., Lin, K., Gu, H., Di Stefano, B.,
1115 Brumbaugh, J., Kim, S.-Y., et al. (2017). Prolonged Mek1/2 suppression impairs the
1116 developmental potential of embryonic stem cells. Nature *548*, 219–223.

1117 40. Di Stefano, B., Luo, E.-C., Haggerty, C., Aigner, S., Charlton, J., Brumbaugh, J., Ji, F.,
1118 Rabano Jiménez, I., Clowers, K.J., Huebner, A.J., et al. (2019). The RNA Helicase DDX6
1119 Controls Cellular Plasticity by Modulating P-Body Homeostasis. Cell Stem Cell *25*, 622–
1120 638.e13.

1121 41. Wu, X., Wu, X., and Xie, W. (2023). Activation, decommissioning, and dememorization:
1122 enhancers in a life cycle. Trends Biochem. Sci. *48*, 673–688.

1123 42. Bonev, B., Mendelson Cohen, N., Szabo, Q., Fritsch, L., Papadopoulos, G.L., Lubling, Y.,
1124 Xu, X., Lv, X., Hugnot, J.-P., Tanay, A., et al. (2017). Multiscale 3D Genome Rewiring
1125 during Mouse Neural Development. Cell *171*, 557–572.e24.

1126 43. Lieberman-Aiden, E., van Berkum, N.L., Williams, L., Imakaev, M., Ragoczy, T., Telling,
1127 A., Amit, I., Lajoie, B.R., Sabo, P.J., Dorschner, M.O., et al. (2009). Comprehensive
1128 mapping of long-range interactions reveals folding principles of the human genome.
1129 Science *326*, 289–293.

1130 44. Álvarez-Villanueva, D., Galán-Palma, L., Bertran, J., Floor, M., Solé, L., Lobo-Jarne, T.,
1131 Maqueda, M., Rajbhandari, R., Marruecos, L., Villà-Freixa, J., et al. (2023). Separation-
1132 of-function mutants reveal the NF-κB-independent involvement of IκBα in the
1133 regulation of stem cell and oncogenic programs. bioRxiv, 2023.06.21.545928.
1134 10.1101/2023.06.21.545928.

1135 45. Guo, Y.-L. (2019). The underdeveloped innate immunity in embryonic stem cells: The
1136 molecular basis and biological perspectives from early embryogenesis. Am. J. Reprod.
1137 Immunol. *81*, e13089.

1138 46. Brena, D., Bertran, J., Porta-de-la-Riva, M., Guillén, Y., Cornes, E., Kukhtar, D., Campos-
1139 Vicens, L., Fernández, L., Pecharroman, I., García-López, A., et al. (2020). Ancestral
1140 function of Inhibitors-of-kappaB regulates Caenorhabditis elegans development. Sci.
1141 Rep. *10*, 16153.

1142 47. Lando, D., Ma, X., Cao, Y., Jartseva, A., Stevens, T.J., Boucher, W., Reynolds, N.,
1143 Montibus, B., Hall, D., Lackner, A., et al. (2024). Enhancer-promoter interactions are
1144 reconfigured through the formation of long-range multiway hubs as mouse ES cells exit
1145 pluripotency. Mol. Cell *84*, 1406–1421.e8.

1146 48. Pantier, R., Tatar, T., Colby, D., and Chambers, I. (2019). Endogenous epitope-tagging of
1147 Tet1, Tet2 and Tet3 identifies TET2 as a naïve pluripotency marker. Life Sci Alliance *2*.
1148 10.26508/lsa.201900516.

1149 49. Sroczynska, P., Lancrin, C., Pearson, S., Kouskoff, V., and Lacaud, G. (2009). In vitro
1150 differentiation of mouse embryonic stem cells as a model of early hematopoietic
1151 development. Methods Mol. Biol. *538*, 317–334.

1152 50. Chen, Q., Luo, W., Veach, R.A., Hickman, A.B., Wilson, M.H., and Dyda, F. (2020).
1153 Structural basis of seamless excision and specific targeting by piggyBac transposase.
1154 Nat. Commun. *11*, 3446.

1155 51. Schneider, C.A., Rasband, W.S., and Eliceiri, K.W. (2012). NIH Image to ImageJ: 25 years
1156 of image analysis. Nat. Methods *9*, 671–675.

1157 52. Ewels, P., Afyounian, E., and Schuster-Boeckler, B.F.K. (2012). TrimGalore: v0. 6.7-DOI
1158 via Zenodo.(Zenodo, 2021). doi: 10.5281/zenodo. 5127899. 2. Langmead, B. & Salzberg,
1159 SL Fast gapped-read alignment with …. Nat. Methods.

1160 53. Langmead, B., and Salzberg, S.L. (2012). Fast gapped-read alignment with Bowtie 2.
1161 Nat. Methods *9*, 357–359.

1162 54. Axtell, M.J. (2013). ShortStack: comprehensive annotation and quantification of small
1163 RNA genes. RNA *19*, 740–751.

1164 55. Danecek, P., Bonfield, J.K., Liddle, J., Marshall, J., Ohan, V., Pollard, M.O., Whitwham,
1165 A., Keane, T., McCarthy, S.A., Davies, R.M., et al. (2021). Twelve years of SAMtools and
1166 BCFtools. Gigascience *10*. 10.1093/gigascience/giab008.

1167 56. Landt, S.G., Marinov, G.K., Kundaje, A., Kheradpour, P., Pauli, F., Batzoglou, S.,
1168 Bernstein, B.E., Bickel, P., Brown, J.B., Cayting, P., et al. (2012). ChIP-seq guidelines and
1169 practices of the ENCODE and modENCODE consortia. Genome Res. *22*, 1813–1831.

1170 57. Ramírez, F., Ryan, D.P., Grüning, B., Bhardwaj, V., Kilpert, F., Richter, A.S., Heyne, S.,
1171 Dündar, F., and Manke, T. (2016). deepTools2: a next generation web server for deep-
1172 sequencing data analysis. Nucleic Acids Res. *44*, W160–W165.

1173 58. Stovner, E.B., and Sætrom, P. (2019). epic2 efficiently finds diffuse domains in ChIP-seq
1174 data. Bioinformatics *35*, 4392–4393.

1175 59. Zhang, Y., Liu, T., Meyer, C.A., Eeckhoute, J., Johnson, D.S., Bernstein, B.E., Nusbaum,
1176 C., Myers, R.M., Brown, M., Li, W., et al. (2008). Model-based analysis of ChIP-Seq
1177 (MACS). Genome Biol. *9*, R137.

1178 60. Zhu, L.J., Gazin, C., Lawson, N.D., Pagès, H., Lin, S.M., Lapointe, D.S., and Green, M.R.
1179 (2010). ChIPpeakAnno: a Bioconductor package to annotate ChIP-seq and ChIP-chip
1180 data. BMC Bioinformatics *11*, 237.

1181 61. Stark, R., Brown, G., and Others (2011). DiffBind: differential binding analysis of ChIP-
1182 Seq peak data. R package version *100*.

1183 62. Gu, Z., Eils, R., Schlesner, M., and Ishaque, N. (2018). EnrichedHeatmap: an
1184 R/Bioconductor package for comprehensive visualization of genomic signal

1185 associations. BMC Genomics *19*, 234.

1186 63. Robinson, J.T., Thorvaldsdóttir, H., Winckler, W., Guttman, M., Lander, E.S., Getz, G.,
1187 and Mesirov, J.P. (2011). Integrative genomics viewer. Nat. Biotechnol. *29*, 24–26.

1188 64. Liao, Y., Smyth, G.K., and Shi, W. (2014). featureCounts: an efficient general purpose
1189 program for assigning sequence reads to genomic features. Bioinformatics *30*, 923–
1190 930.

1191 65. Love, M.I., Huber, W., and Anders, S. (2014). Moderated estimation of fold change and
1192 dispersion for RNA-seq data with DESeq2. Genome Biol. *15*, 550.

1193 66. Zhu, A., Ibrahim, J.G., and Love, M.I. (2019). Heavy-tailed prior distributions for
1194 sequence count data: removing the noise and preserving large differences.
1195 Bioinformatics *35*, 2084–2092.

1196 67. Benjamini, Y., and Hochberg, Y. (1995). Controlling the False Discovery Rate: A Practical
1197 and Powerful Approach to Multiple Testing. J. R. Stat. Soc. Series B Stat. Methodol. *57*,
1198 289–300.

1199 68. Garcia-Prieto, C.A., Álvarez-Errico, D., Musulen, E., Bueno-Costa, A., N. Vazquez, B.,
1200 Vaquero, A., and Esteller, M. (2022). Validation of a DNA methylation microarray for
1201 285,000 CpG sites in the mouse genome. Epigenetics *17*, 1677–1685.

1202 69. Ashburner, M., Ball, C.A., Blake, J.A., Botstein, D., Butler, H., Cherry, J.M., Davis, A.P.,
1203 Dolinski, K., Dwight, S.S., Eppig, J.T., et al. (2000). Gene ontology: tool for the
1204 unification of biology. The Gene Ontology Consortium. Nat. Genet. *25*, 25–29.

1205 70. Kanehisa, M., and Goto, S. (2000). KEGG: kyoto encyclopedia of genes and genomes.
1206 Nucleic Acids Res. *28*, 27–30.

1207 71. Martens, M., Ammar, A., Riutta, A., Waagmeester, A., Slenter, D.N., Hanspers, K., A
1208 Miller, R., Digles, D., Lopes, E.N., Ehrhart, F., et al. (2021). WikiPathways: connecting
1209 communities. Nucleic Acids Res. *49*, D613–D621.

1210 72. Hu, S., Metcalf, E., Mahat, D.B., Chan, L., Sohal, N., Chakraborty, M., Hamilton, M.,
1211 Singh, A., Singh, A., Lees, J.A., et al. (2022). Transcription factor antagonism regulates
1212 heterogeneity in embryonic stem cell states. Mol. Cell *82*, 4410–4427.e12.

1213 73. Korotkevich, G., Sukhov, V., Budin, N., Shpak, B., Artyomov, M.N., and Sergushichev, A.
1214 (2021). Fast gene set enrichment analysis. bioRxiv, 060012. 10.1101/060012.

1215 74. Zhou, W., Triche, T.J., Jr, Laird, P.W., and Shen, H. (2018). SeSAMe: reducing artifactual
1216 detection of DNA methylation by Infinium BeadChips in genomic deletions. Nucleic
1217 Acids Res. *46*, e123.

1218 75. Hänzelmann, S., Castelo, R., and Guinney, J. (2013). GSVA: gene set variation analysis
1219 for microarray and RNA-seq data. BMC Bioinformatics *14*, 7.

1220 76. Bleckwehl, T., Crispatzu, G., Schaaf, K., Respuela, P., Bartusel, M., Benson, L., Clark, S.J.,

1221 Dorighi, K.M., Barral, A., Laugsch, M., et al. (2021). Enhancer-associated H3K4
1222 methylation safeguards in vitro germline competence. Nat. Commun. *12*, 5771.

Figure 1

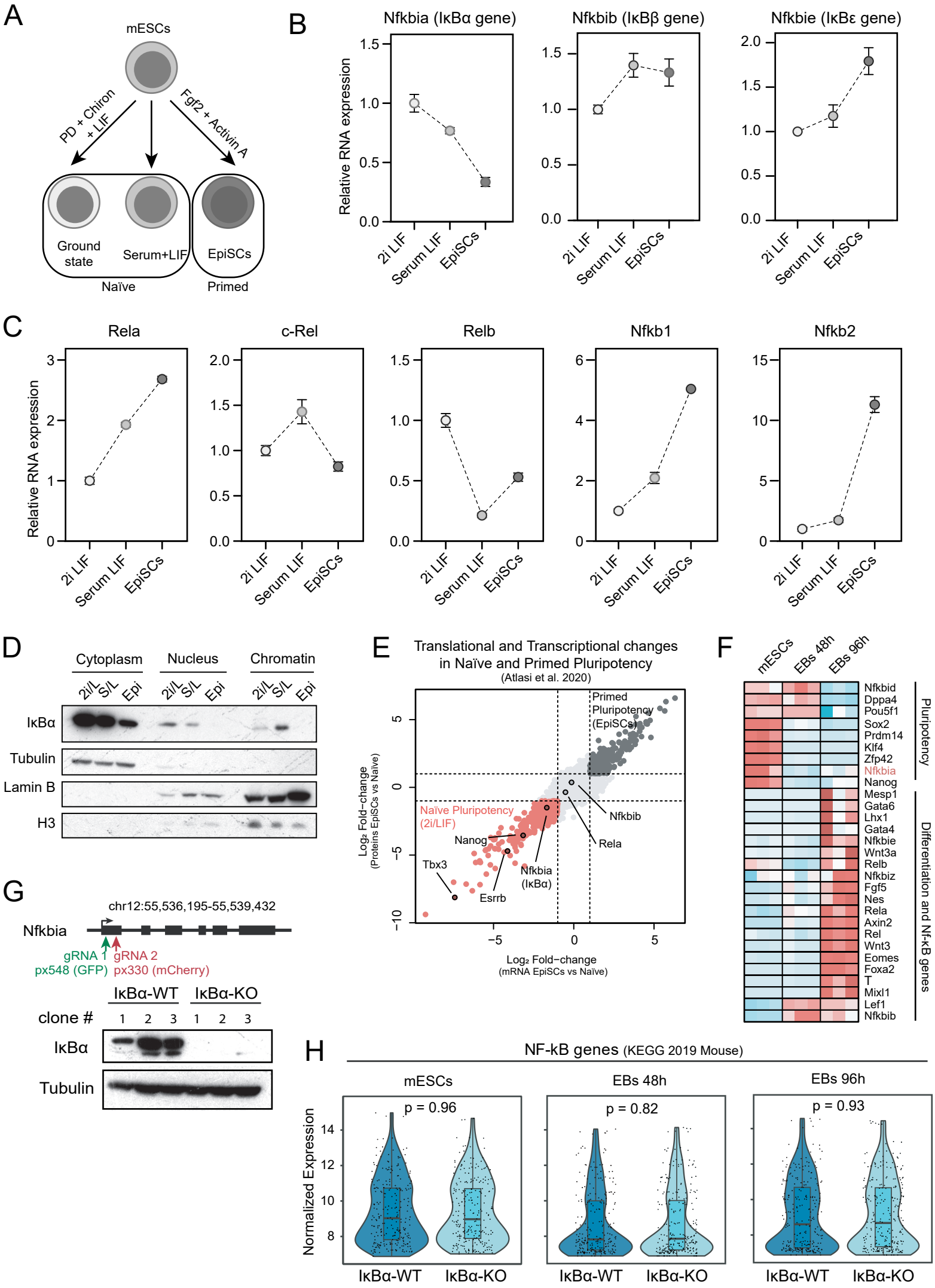
A
mESCs
PD + Chiron + LIF
Fgf2 + Activin A
Ground state
Serum+LIF
EpiSCs
Naïve
Primed
B
Nfkbia (IκBα gene)
Nfkbib (IκBβ gene)
Nfkbie (IκBε gene)
Relative RNA expression
2i LIF
Serum LIF
EpiSCs
C
Rela
c-Rel
Relb
Nfkb1
Nfkb2
Relative RNA expression
2i LIF
Serum LIF
EpiSCs
D
Cytoplasm
Nucleus
Chromatin
2i/L
S/L
Epi
IκBα
Tubulin
Lamin B
H3
E
Translational and Transcriptional changes in Naïve and Primed Pluripotency
(Atlasi et al. 2020)
Primed Pluripotency (EpiSCs)
Naïve Pluripotency (2i/LIF)
Nfkbib
Rela
Nanog
Tbx3
Nfkbia (IκBα)
Esrrb
Log₂ Fold−change (Proteins EpiSCs vs Naïve)
Log₂ Fold−change (mRNA EpiSCs vs Naïve)
F
mESCs
EBs 48h
EBs 96h
Nfkbid
Dppa4
Pou5f1
Sox2
Prdm14
Klf4
Zfp42
Nfkbia
Nanog
Mesp1
Gata6
Lhx1
Gata4
Nfkbie
Wnt3a
Relb
Nfkbiz
Fgf5
Nes
Rela
Axin2
Rel
Wnt3
Eomes
Foxa2
T
Mixl1
Lef1
Nfkbib
Pluripotency
Differentiation and Nf-kB genes
G
chr12:55,536,195-55,539,432
Nfkbia
gRNA 1
gRNA 2
px548 (GFP)
px330 (mCherry)
IκBα-WT
IκBα-KO
clone #
1 2 3 1 2 3
IκBα
Tubulin
H
NF-kB genes (KEGG 2019 Mouse)
mESCs
EBs 48h
EBs 96h
p = 0.96
p = 0.82
p = 0.93
Normalized Expression
IκBα-WT
IκBα-KO

Figure 2

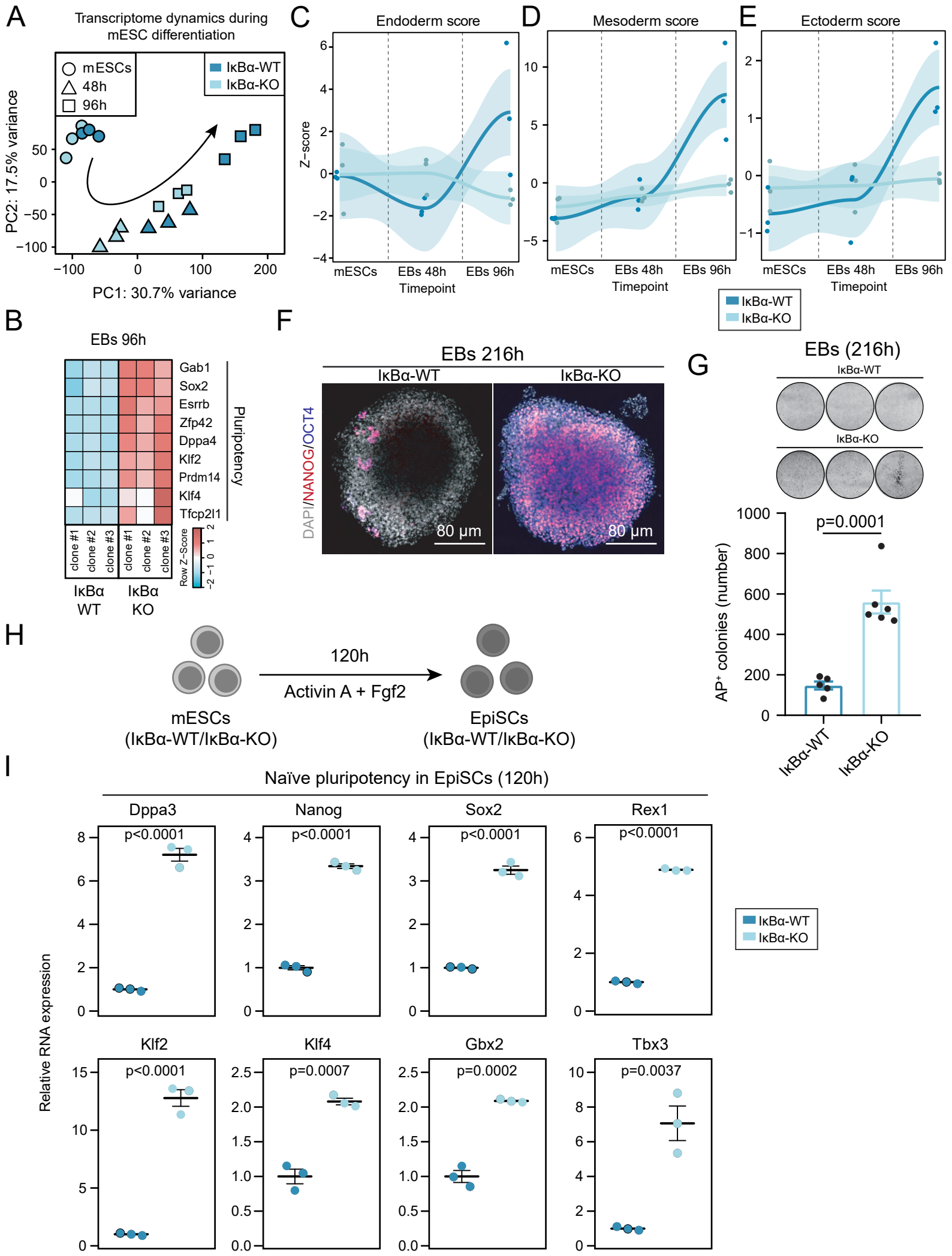
A
Transcriptome dynamics during mESC differentiation
mESCs
48h
96h
IκBα-WT
IκBα-KO
PC2: 17.5% variance
PC1: 30.7% variance
B
EBs 96h
Gab1
Sox2
Esrrb
Zfp42
Dppa4
Klf2
Prdm14
Klf4
Tfcp2l1
Pluripotency
clone #1
clone #2
clone #3
Row Z-Score
IκBα WT
IκBα KO
C
Endoderm score
D
Mesoderm score
E
Ectoderm score
Z-score
mESCs
EBs 48h
EBs 96h
Timepoint
F
EBs 216h
IκBα-WT
IκBα-KO
DAPI/NANOG/OCT4
80 µm
G
EBs (216h)
p=0.0001
AP⁺ colonies (number)
H
120h
Activin A + Fgf2
mESCs
(IκBα-WT/IκBα-KO)
EpiSCs
(IκBα-WT/IκBα-KO)
I
Naïve pluripotency in EpiSCs (120h)
Dppa3
Nanog
Sox2
Rex1
Klf2
Klf4
Gbx2
Tbx3
p<0.0001
p=0.0007
p=0.0002
p=0.0037
Relative RNA expression

Figure 3

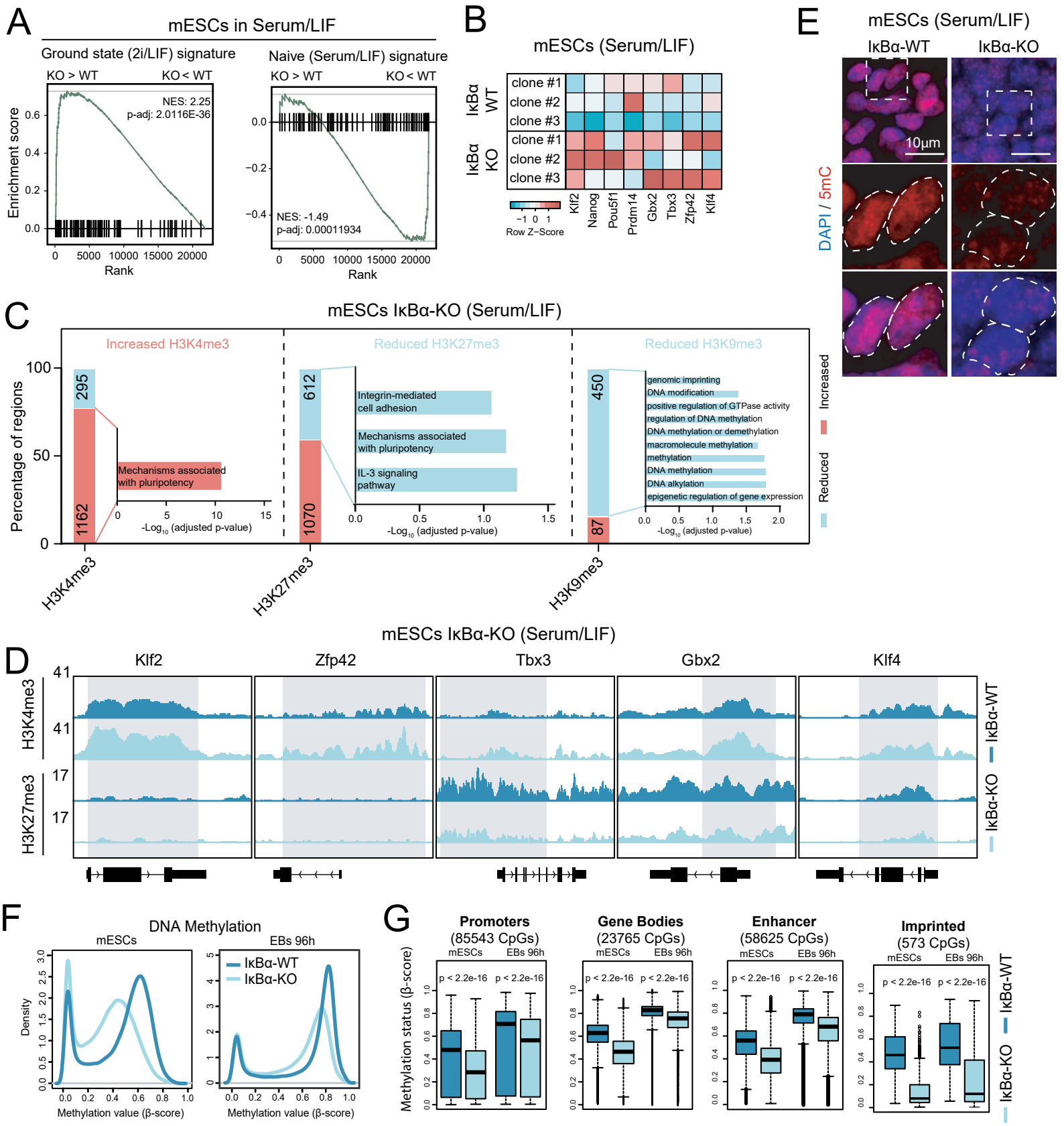
A
mESCs in Serum/LIF
Ground state (2i/LIF) signature
Naive (Serum/LIF) signature
KO > WT
KO < WT
NES: 2.25
p-adj: 2.0116E-36
NES: -1.49
p-adj: 0.00011934
Enrichment score
Rank
B
mESCs (Serum/LIF)
IκBα WT
IκBα KO
clone #1
clone #2
clone #3
Klf2
Nanog
Pou5f1
Prdm14
Gbx2
Tbx3
Zfp42
Klf4
Row Z-Score
E
mESCs (Serum/LIF)
IκBα-WT
IκBα-KO
10μm
DAPI / 5mC
C
mESCs IκBα-KO (Serum/LIF)
Increased H3K4me3
Reduced H3K27me3
Reduced H3K9me3
Percentage of regions
295
1162
612
1070
450
87
Mechanisms associated with pluripotency
Integrin-mediated cell adhesion
Mechanisms associated with pluripotency
IL-3 signaling pathway
genomic imprinting
DNA modification
positive regulation of GTPase activity
regulation of DNA methylation
DNA methylation or demethylation
macromolecule methylation
methylation
DNA methylation
DNA alkylation
epigenetic regulation of gene expression
-Log10 (adjusted p-value)
Increased
Reduced
H3K4me3
H3K27me3
D
mESCs IκBα-KO (Serum/LIF)
Klf2
Zfp42
Tbx3
Gbx2
Klf4
IκBα-WT
IκBα-KO
F
DNA Methylation
mESCs
EBs 96h
IκBα-WT
IκBα-KO
Density
Methylation value (β-score)
G
Promoters
(85543 CpGs)
Gene Bodies
(23765 CpGs)
Enhancer
(58625 CpGs)
Imprinted
(573 CpGs)
mESCs
EBs 96h
p < 2.2e-16
Methylation status (β-score)
IκBα-WT
IκBα-KO

Figure 4

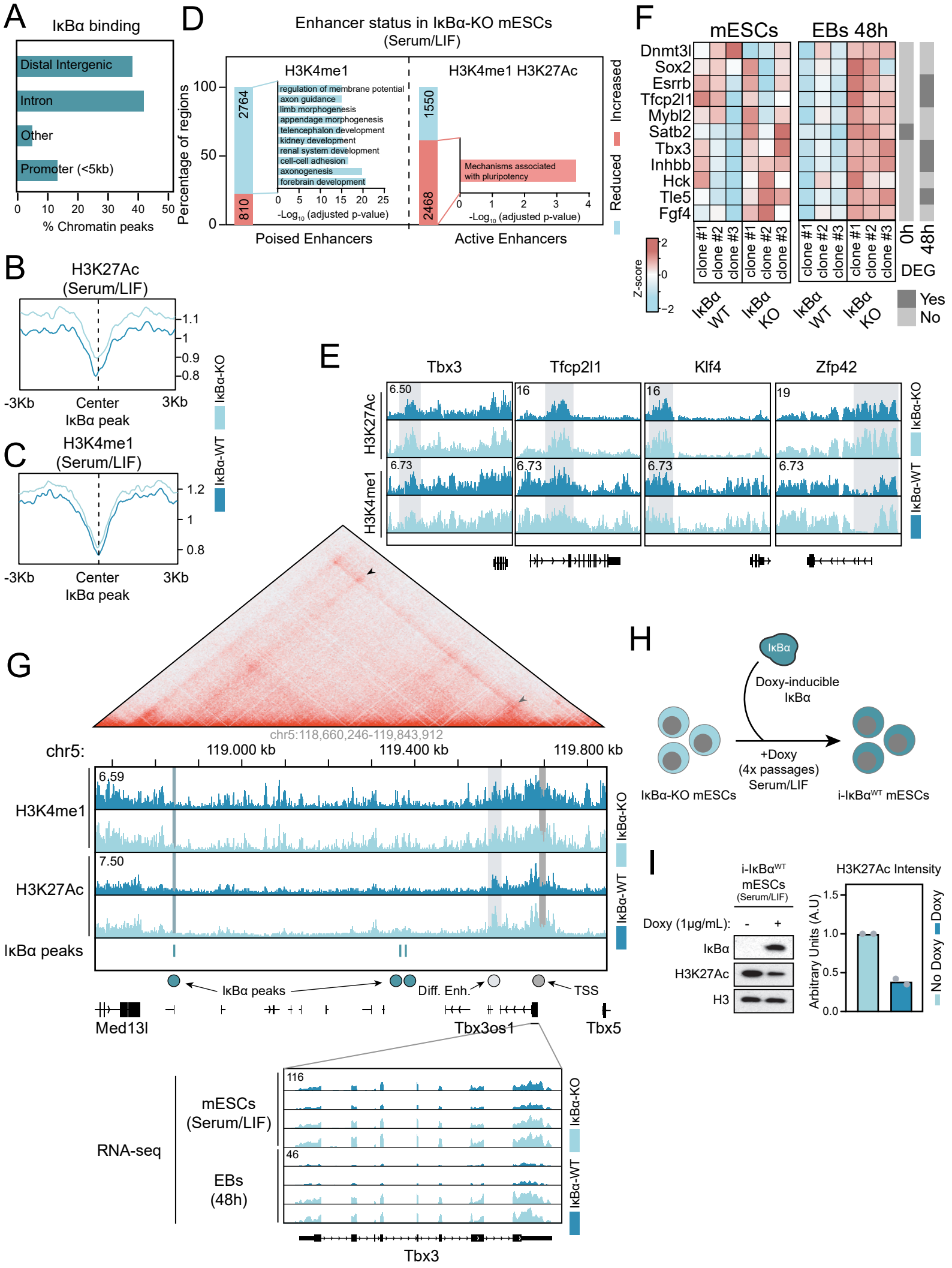
A
IκBα binding
Distal Intergenic
Intron
Other
Promoter (<5kb)
% Chromatin peaks
B
H3K27Ac (Serum/LIF)
-3Kb
Center IκBα peak
3Kb
IκBα-KO
IκBα-WT
C
H3K4me1 (Serum/LIF)
D
Enhancer status in IκBα-KO mESCs (Serum/LIF)
H3K4me1
H3K4me1 H3K27Ac
Percentage of regions
2764
810
1550
2468
regulation of membrane potential
axon guidance
limb morphogenesis
appendage morphogenesis
telencephalon development
kidney development
renal system development
cell-cell adhesion
axonogenesis
forebrain development
Mechanisms associated with pluripotency
-Log10 (adjusted p-value)
Poised Enhancers
Active Enhancers
Increased
Reduced
E
Tbx3
Tfcp2l1
Klf4
Zfp42
H3K27Ac
H3K4me1
6.50
16
16
19
6.73
6.73
6.73
6.73
F
mESCs
EBs 48h
Dnmt3l
Sox2
Esrrb
Tfcp2l1
Mybl2
Satb2
Tbx3
Inhbb
Hck
Tle5
Fgf4
clone #1
clone #2
clone #3
Z-score
IκBα WT
IκBα KO
0h
48h
DEG
Yes
No
G
chr5:118,660,246-119,843,912
chr5:
119.000 kb
119.400 kb
119.800 kb
H3K4me1
H3K27Ac
IκBα peaks
6.59
7.50
IκBα-KO
IκBα-WT
IκBα peaks
Diff. Enh.
TSS
Med13l
Tbx3os1
Tbx5
RNA-seq
mESCs (Serum/LIF)
EBs (48h)
116
46
Tbx3
H
IκBα
Doxy-inducible IκBα
+Doxy (4x passages) Serum/LIF
IκBα-KO mESCs
i-IκBα^WT mESCs
I
i-IκBα^WT mESCs (Serum/LIF)
Doxy (1μg/mL):
-
+
IκBα
H3K27Ac
H3
H3K27Ac Intensity
Arbitrary Units (A.U)
No Doxy
Doxy

Figure 5

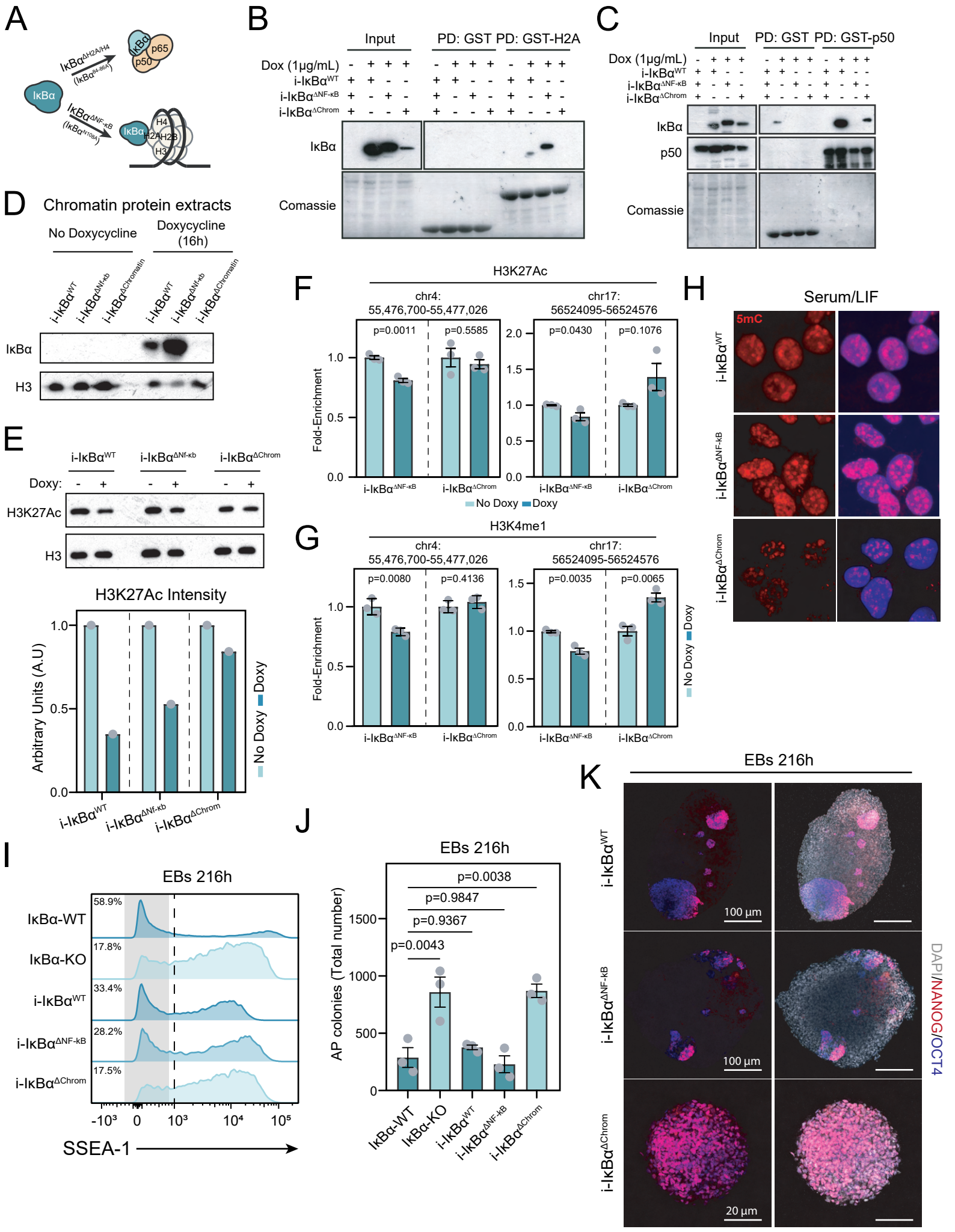
A
IκBα
IκBα^ΔH2A/H4 (IκBα^84-86A)
IκBα
p65
p50
IκBα^ΔNF-κB (IκBα^N108A)
IκBα
H4
H2A
H2B
H3
B
Input
PD: GST
PD: GST-H2A
Dox (1μg/mL)
i-IκBα^WT
i-IκBα^ΔNF-κB
i-IκBα^ΔChrom
IκBα
Comassie
C
Input
PD: GST
PD: GST-p50
Dox (1μg/mL)
i-IκBα^WT
i-IκBα^ΔNF-κB
i-IκBα^ΔChrom
IκBα
p50
Comassie
D
Chromatin protein extracts
No Doxycycline
Doxycycline (16h)
i-IκBα^WT
i-IκBα^ΔNf-κb
i-IκBα^ΔChromatin
IκBα
H3
E
i-IκBα^WT
i-IκBα^ΔNf-κb
i-IκBα^ΔChrom
Doxy:
H3K27Ac
H3
H3K27Ac Intensity
Arbitrary Units (A.U)
No Doxy
Doxy
F
H3K27Ac
chr4: 55,476,700-55,477,026
chr17: 56524095-56524576
p=0.0011
p=0.5585
p=0.0430
p=0.1076
Fold-Enrichment
No Doxy
Doxy
G
H3K4me1
chr4: 55,476,700-55,477,026
chr17: 56524095-56524576
p=0.0080
p=0.4136
p=0.0035
p=0.0065
Fold-Enrichment
No Doxy
Doxy
H
Serum/LIF
5mC
i-IκBα^WT
i-IκBα^ΔNF-κB
i-IκBα^ΔChrom
I
EBs 216h
IκBα-WT
IκBα-KO
i-IκBα^WT
i-IκBα^ΔNF-κB
i-IκBα^ΔChrom
58.9%
17.8%
33.4%
28.2%
17.5%
SSEA-1
J
EBs 216h
p=0.0038
p=0.9847
p=0.9367
p=0.0043
AP colonies (Total number)
IκBα-WT
IκBα-KO
i-IκBα^WT
i-IκBα^ΔNF-κB
i-IκBα^ΔChrom
K
EBs 216h
i-IκBα^WT
i-IκBα^ΔNF-κB
i-IκBα^ΔChrom
100 μm
100 μm
20 μm
DAPI/NANOG/OCT4

Figure 6

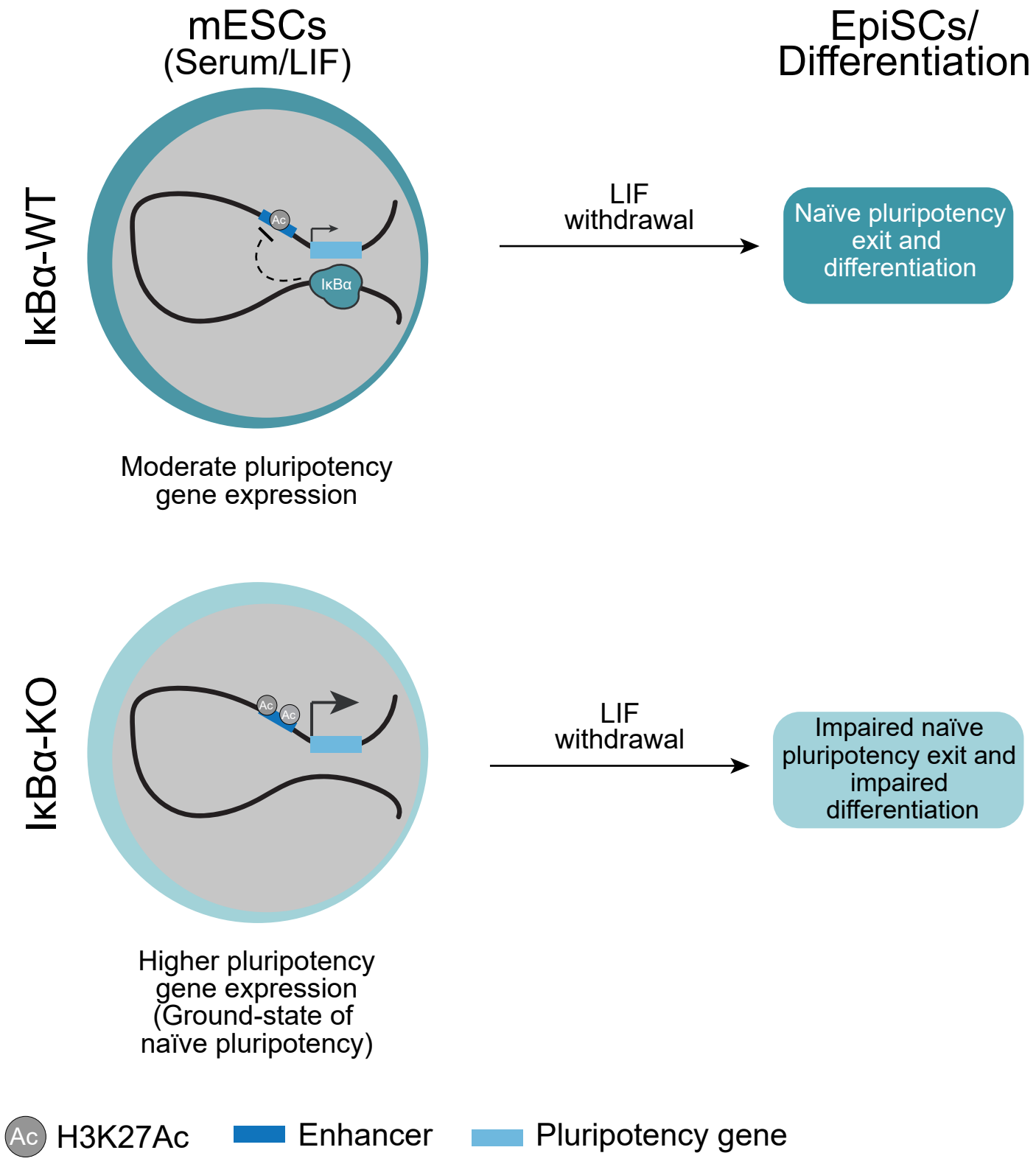
mESCs
(Serum/LIF)
EpiSCs/
Differentiation
IκBα-WT
Ac
IκBα
LIF
withdrawal
Naïve pluripotency
exit and
differentiation
Moderate pluripotency
gene expression
IκBα-KO
Ac
Ac
LIF
withdrawal
Impaired naïve
pluripotency exit and
impaired
differentiation
Higher pluripotency
gene expression
(Ground-state of
naïve pluripotency)
Ac H3K27Ac
Enhancer
Pluripotency gene